Chapter 1

Brillouin Scattering in Optical Fibers and Its Application to Distributed Sensors

Weiwen Zou, Xin Long and Jianping Chen

Additional information is available at the end of the chapter

http://dx.doi.org/10.5772/59145

1. Introduction

Brillouin based distributed optical fiber sensors have been studied for more than two decades because they have incomparable abilities over the pointed or multiplexed fiber-optic sensors based on fiber Bragg grating and/or inline Fabry-Perot resonator. They originated from the intrinsic fiber-optic nonlinearity in optical fibers, i.e. Brillouin scattering, and have many distinguished advantages, such as high accuracy due to the frequency revolved interrogation, multiple sensitivities of measurands (strain, temperature etc.), no dead zones of sensing location due to the distributed sensing ability, and immunity to the electro-magnetic interference. Nowadays, they have been thought as great potentials in industrial applications to smart materials and smart structures.

This chapter introduces the basic principle and recent advances of Brillouin scattering in optical fibers. The working mechanism, different interrogation techniques, difficulty or challenge of the sensing ability, and recent breakthroughs of Brillouin based distributed optical fiber sensors are demonstrated, respectively.

2. Brillouin scattering in optical fibers

2.1. Principle

Light scattering phenomena in optical fibers occur regardless of how intense the incident optical power is. They can be basically categorized into two groups, i.e. spontaneous scattering and stimulated scattering[1]. Spontaneous scattering refers to the process under conditions such that the material properties are unaffected by the presence of the incident optical fields.

For input optical fields of sufficient intensities spontaneous scattering becomes quite intense and stimulated scattering starts. The nature of the stimulated scattering process grossly modifies the optical properties of the material system and vice versa. Spontaneous and stimulated scattering in optical fibers are composed of Rayleigh, Raman, and Brillouin scattering processes. Each scattering process is always present in optical fibers since no fiber is free from microscopic defects or thermal fluctuations which originate the three processes. For a monochromatic incident lightwave of frequency f_0 at $\lambda_{0=}$~1550 nm (telecom wavelength), three processes are schematically described by the spectrum of the scattered light as shown in Fig. 1. The components, whose frequency is beyond f_0, correspond to anti-Stokes while those below f_0 correspond to Stokes.

Brillouin scattering is a "photon-phonon" interaction as annihilation of a pump photon creates a Stokes photon and a phonon simultaneously. The created phonon is the vibrational modes of atoms, also called a propagation density wave or an acoustic phonon/wave. In a silica-based optical fiber, Brillouin Stokes wave propagates dominantly backward [2] although very partially forward[3]. The frequency (~9-11 GHz) of Stokes photon at ~1550-nm wavelength is in quantity dramatically different from or smaller by three orders of magnitude than Raman scattering (see Fig. 1) and is dominantly down-shifted due to Doppler shift associated with the forward movement of created acoustic phonons. In a polymer optical fiber, the frequency is ~2-3 GHz due to the different phonon property[4].

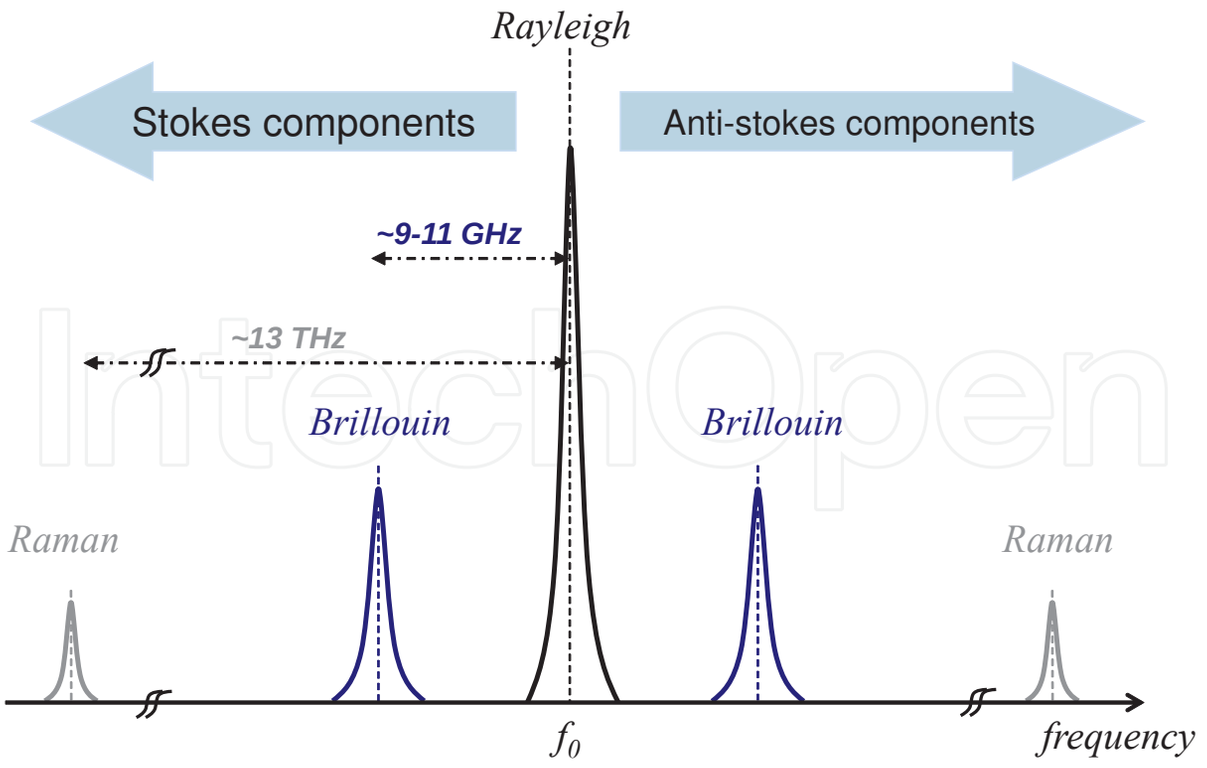

Figure 1. Schematic spectrum of scattered light resulting from three scattering processes in optical fibers.

http://dx.doi.org/10.5772/59145

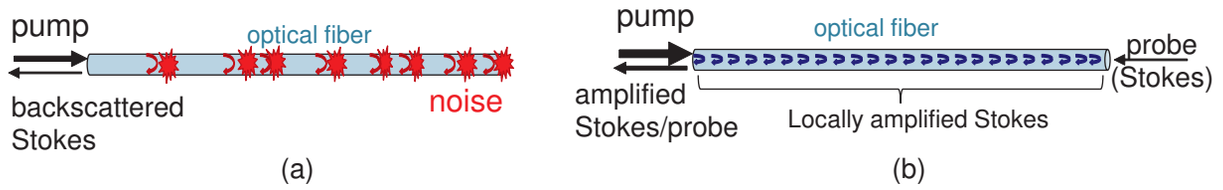

Figure 2. Comparison of (a) spontaneous Brillouin scattering (SpBS) and (b) stimulated Brillouin scattering (SBS) in optical fibers.

Figure 2 illustrates the difference between spontaneous Brillouin scattering (SpBS) and stimulated Brillouin scattering (SBS) in optical fibers. In principle, the SpBS (see Fig. 2(a)) is started from a noise fluctuation and influences the pump wave (E_p); the SBS (see Fig. 2(b)) occurs when the pump power for SpBS is beyond the so-called Brillouin threshold value (P_{th}) or when two coherent waves with a frequency difference equivalent to the phonon's frequency are counter-propagated. Brillouin scattering dynamics in optical fibers are generally governed by the following coupling equations [5, 6]:

$$\left(\frac{1}{v_g}\frac{\partial}{\partial t}+\frac{\partial}{\partial z}\right)E_p=-\frac{\alpha}{2}E_p+i\kappa_1\rho E_s, \tag{1}$$

$$\left(\frac{1}{v_g}\frac{\partial}{\partial t}-\frac{\partial}{\partial z}\right)E_s=-\frac{\alpha}{2}E_s+i\kappa_1\rho^* E_s, \tag{2}$$

$$\left(+\frac{\partial}{\partial t}+\frac{\Gamma_B}{2}+2\pi i\nu_B\right)\rho=i\kappa_2 E_p E_s^*+N, \tag{3}$$

where E_p and E_s stand for the normalized slowly-varying fields of pump and Stokes (or probe) waves, respectively; and $P_p=|E_p|^2$ and $P_s=|E_s|^2$ correspond to their optical powers; ρ denotes the acoustic (or phonon) field in terms of the material density distribution; N represents the random fluctuation or white noise in position and time [5]; v_g is the group light velocity in the fiber; α is the fiber's propagation loss; Γ_B is the damping rate of the acoustic wave, which equals to the reciprocal of the phonon's lifetime ($1/\Gamma_B=\tau_\rho=$~10 ns) and is related to the acoustic linewidth ($\Delta\nu_B=\Gamma_B/\pi$) [7]; κ_1 and κ_2 are the coupling coefficients among E_p, E_s, and ρ. If SpBS is considered, it is reasonable to assume E_s is sufficiently small so that the second term of N dominates in the right side of Eq. (3). In contrast, the first term of $i\kappa_2 E_p E_s^*$ dominates for SBS.

Taken into account the SBS power transfer between P_p and P_s under the assistance of the acoustic wave and the so-called acousto-optic effect, Eqs. (1-3) can be rewritten as

$$\left(\frac{1}{v_g}\frac{\partial}{\partial t}+\frac{\partial}{\partial z}+\alpha\right)P_p=-g(\nu)P_pP_s, \tag{4}$$

$$\left(\frac{1}{v_g}\frac{\partial}{\partial t}-\frac{\partial}{\partial z}+\alpha\right)P_s=+g(\nu)P_pP_s, \tag{5}$$

where the sign difference between the right hands of Eq. (4) and Eq. (5) means that the pump power is reduced or depleted but the probe (Stokes) power is increased or amplified.

g(ν) is called Brillouin gain spectrum (BGS), the key phraseology to represent Brillouin scattering in optical fibers. It denotes the spectral details of the light amplification from strong pump wave to weak counter-propagating probe/Stokes wave in SBS or those of the noise-initialized scattered phonons in SpBS. The BGS is generally expressed by [8-10]

$$g(\nu)=\sum_l g^{(l)}(\nu), \tag{6}$$

$$g^{(l)}(\nu)=\left\{g_{B0}\cdot\frac{\nu_B\cdot\Delta\nu_B}{\nu_{ac}{}^{(l)}\cdot\Delta\nu_{ac}{}^{(l)}}\right\}\cdot\left\{\frac{(\Delta\nu_{ac}{}^{(l)}/2)^2}{[\nu-(f_0-\nu_{ac}{}^{(l)})]^2+(\Delta\nu_{ac}{}^{(l)}/2)^2}\right\}\cdot\left\{\frac{1}{A_{ao}^{(l)}}\right\}, \tag{7}$$

where Eq. (6) means that the BGS is the summation of all the longitudinal acoustic modes' gain spectra and Eq. (7) corresponds to the *l*th-order one assigned the subscript of "*l*". In Eq. (7), $\Delta\nu_{ac}{}^{(l)}$ is the *l*th-order linewidth or full width at half magnitude (FWHM) which can be assumed to be approximately the same for all the acoustic modes; $\nu_{ac}{}^{(l)}$ is the effective acoustic velocity; $A_{ao}{}^{(l)}$ (in μm^2) is the so-called acousto-optic effective area of the *l*th-order one. $\nu_{ac}{}^{(l)}$ and $A_{ao}{}^{(l)}$ are qualitatively different among all acoustic modes.

There are two basic methods to theoretically and numerically analyze the BGS in optical fibers [8, 11]. One method [11] is based on Bessel or modified Bessel functions for optical fibers with regular geometric and dopant distribution, such as step-index optical fibers. The other one [8] is called two-dimensional finite-element-method (2D-FEM) modal analysis of BGS for optical fibers with complicated or arbitrary distribution. The 2D-FEM modal analysis has been used to study a Panda-type polarization-maintaining optical fiber (PMF) [8], a SMF with arbitrary residual stress [12], a *w*-shaped triple-layer fiber [13], or optical fibers with non-uniform optical/acoustic profiles such as solid or microsctrucuted photonic crystal fibers (PCF) [14-21].

The contribution of the fundamental acoustic mode to the entire BGS is basically dominant, which has a Lorentzian feature as schematically depicted in Fig. 3(a). Besides, it modulates the refractive index of optical fiber and changes the group velocity of optical fields in a profile shown in the inset of Fig. 3(a), which has been adopted for Brillouin slow or fast light[22, 23].

http://dx.doi.org/10.5772/59145

There are three basic parameters of Brillouin frequency shift (BFS, ν_B), Brillouin gain peak (g_{B0}), and Brillouin linwidth ($\Delta\nu_B$) in the main-peak BGS (i.e. the fundamental acoustic mode or l=1 in Eq. (7)). ν_B is defined as

$$\nu_B \equiv \nu_{ac}^{(1)} = \frac{2}{\lambda_0} \cdot n_{eff} \cdot V_a, \tag{8}$$

where λ_0 is the light wavelength ($\lambda_0=c/f_0$ with c the light speed in vacuum), n_{eff} is the effective refractive index of the fiber, and V_a is the effective acoustic velocity of the fundamental acoustic mode. n_{eff} and V_a in Eq. (8) as well as $A_{ao}^{(l)}$ in Eq. (7) are all determined by the respective waveguide structures of the optical modes (n_0 and n_1) and those of the longitudinal acoustic modes (V_{l1}, V_{l0}), relative to the silica dopant materials and distributions in the cross section [24]. Figure 3(b) illustrates a simple example of step-index single-mode optical fiber (SMF), even for which the BGS comprises of several (typically, four) longitudinal acoustic modes due to the different contrast of optical and acoustic waveguides [8, 11]. The measured BGS of the SMF and a high-delta nonlinear optical fiber at 1550nm are depicted in Fig. 3(c)[13]. It is worth noting that ν_B in optical fibers suffers strong influence from the residual elastic and inelastic strains induced by different draw tensions during fiber fabrication[12].

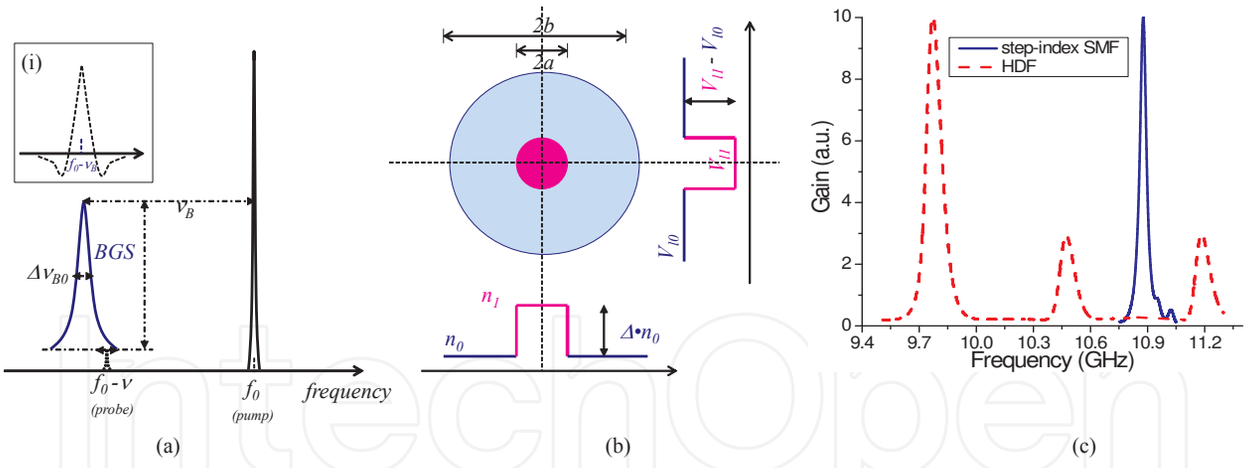

Figure 3. (a) Brillouin gain spectrum (BGS) in optical fibers. The inset "i" denotes the change of group velocity of optical fields. (b) Cross section of a step-index SMF. $\Delta=(n_1-n_0)/n_0$ is the relative index difference between the core (n_1) and the cladding (n_0). (c) Measured BGS of a step-index SMF (solid curve) and of a 17.0-mol% high-delta fiber (dashed curve). (Fig. 3(c) after Ref. [13]; © 2008 OSA.)

g_{B0} in Eq. (7) is determined by

$$g_{B0} = \frac{4\pi {n_{eff}}^8 {p_{12}}^2}{{\lambda_0}^3 \rho_0 c \nu_B \Delta\nu_{B0}}, \tag{9}$$

where ρ_0 is the density of silica glass (~2202 kg/m^3) and p_{12} the photo-elastic constant (~0.271). In most silica-based fibers, the peak gain value of g_{B0} lies in the range of 1.5~3× 10^{-11} m/W [25].

$\Delta\nu_{B0}$ in silica optical fibers with a typical value of 30~40 MHz is characteristic of SpBS. However, in the SBS process, it was theoretically proved that $\Delta\nu_B$ strongly depends on the pump power, which is expressed as follows [5, 26]:

$$\Delta\nu_B = \Delta\nu_{B0}\sqrt{\frac{\ln 2}{G_s}}, \tag{10}$$

where G_s is the single pass gain experienced by the weak probe wave from the strong pump wave, defined by

$$G_s = \frac{g_{B0}P_{pump}L_{eff}}{K \cdot A_{\text{eff}}^{ao}}, \tag{11}$$

where K (=1~2) is a polarization factor (=2 for a complete polarization scrambling process), L_{eff}=[1-exp(-αL)]/α is the effective length of the fiber with α the optical loss (m^{-1}) and L the fiber length, P_{pump} the pump power, and $A_{\text{eff}}^{\text{ao}}$=$A_{ao}^{(1)}$ is the acoustic-optic effective area of the fundamental acoustic mode. It is noted that the exponential (G_e) or logarithmic (G_{dB}, *in dB*) gain of the weak probe power (P_{probe}) are presented by

$$G_e = \frac{\Delta P_{probe}}{P_{probe}} = \exp(G_s) - 1, \tag{12}$$

$$G_{dB} = 10\log_{10}(G_e) \approx 4.342G_s. \tag{13}$$

Eq. (13) is valid when G_e>>1.

From Eq. (10), one could estimate that the linewidth goes gradually to zero for very high gain, which can be obtained by either increasing the pump power or the interaction length of the fiber (see Eq. (11)). A zero linewidth corresponds to acoustic oscillation with an infinite time. However, pump depletion always occurs when the single pass gain (G_s) increases, which results in a limited effective single pass gain and in turn leads to a finite linewidth instead of zero one.

The experimental characterization of the phenomenon of the Brillouin linwidth's narrowing in three SMFs are depicted in Fig. 4 [27]. When the pump power is intensified to a high value of above ~24 dBm (~250 mW), the Brillouin main-peak linewidth of 180-m-long SMF becomes increasing. This is because the pump power depletes much faster than its contribution to the single-pass gain G_s since the probe wave experiences an amplification of more than G_{dB}=20 dB

http://dx.doi.org/10.5772/59145

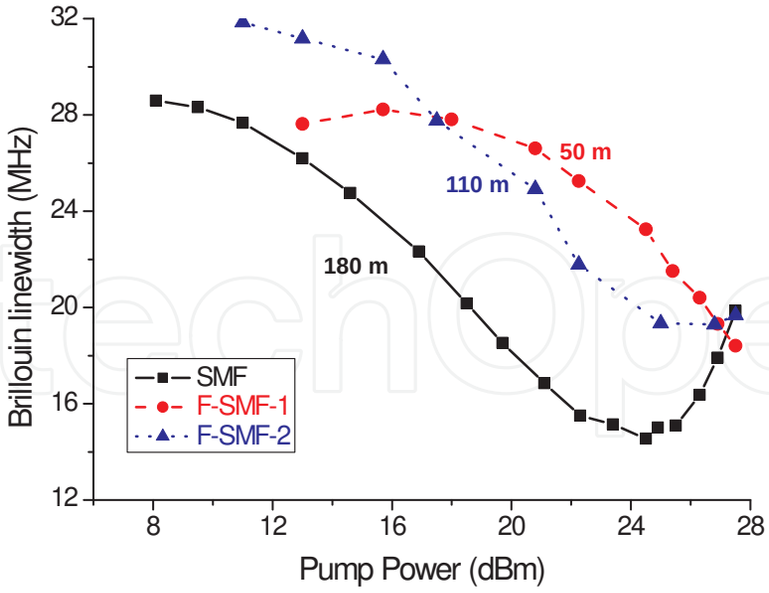

Figure 4. Measured Brillouin linewidth in three SMF varying with increase of Brillouin pump power. F-SMF denotes a SMF with pure-silica core and F-doped-silica cladding. (After Ref. [27]; © 2008 OSA.)

for a greater pump power than ~24 dBm. From the other point of view, during the pump-probe-based BGS measurement, which will be described later, the Brillouin probe wave with a down-shifted frequency of just ν_B feels more significantly the depletion of the pump power than the one with a downshifted frequency of a finite offset from ν_B. More details of the effect of pump depletion in SBS will be demonstrated in **Section 2.3**.

From Eq. (11), one can derivate the so-called pump threshold value of SBS originating from SpBS (also called Brillouin generator). It is given by

$$P_{th} = \kappa \frac{A_{\text{eff}}^{ao}}{L_{eff}} \frac{K}{g_{B0}}, \tag{14}$$

where κ is a numerical factor (=~21) [28] that may change in terms of the fiber length [29]. If a long-enough SMF is considered, α=0.2 dB/km (or 0.046 /km) meaning L_{eff}=21.7 km. $A_{\text{eff}}^{ao} \approx A_{\text{eff}}$=100 μm^2 and g_{B0}=2× 10^{-11} m/W. For a perfectly-linearized pump wave, $P_{\text{th}} \approx$ 3.2 mW; for a completely polarization-scrambled pump wave, $P_{\text{th}} \approx$ 4.6 mW.

2.2. Experimental characterization

The experimental characterization of BGS in optical fibers can be implemented by two individual ways that depend on which principle of SpBS or SBS is based on. The SpBS based configuration is illustrated in Fig. 5(a). A pump wave is amplified by an erbium doped fiber amplifier (EDFA) and its polarization is optimized by a polarization controller (PC), scrambled by a polarization scrambler (PS) or switched by a polarization switcher (PSW). It is launched through an optical coupler or circulator into the fiber under test (FUT). A weak Stokes wave

with downshifted frequency around ν_B is backscattered towards the coupler/circulator and can be detected by three different schemes, which are depicted in Fig. 5(b). First, an optical filter (Etalon, Fabry-Perot filter or FBG) is inserted before a photo-detector (PD) so as to eliminate the influence of Rayleigh scattering on Stokes wave and spectrally analyzed by an electrical spectrum analyzer (ESA) [2, 30]. Second, Stokes wave is optically mixed with a part of the pump wave (serving as an optical oscillator) and then detected or heterodyne-detected by a high-speed PD or a high-speed balanced PD, which is directed to the ESA [31]. Third, heterodyne detection can be carried out at an intermediate frequency (IF) range by tuning the frequency of the optical oscillator or further using of a local microwave (RF) oscillator before ESA [32].

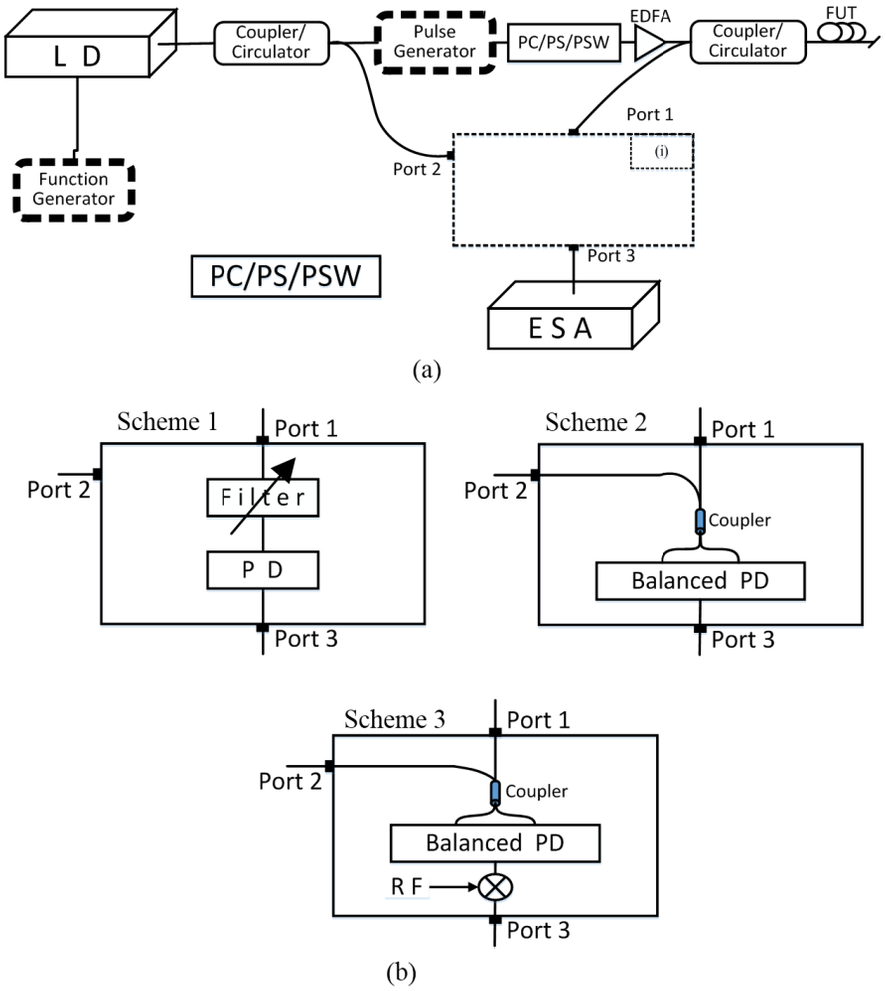

Figure 5. Experimental setup of BGS measurement based on spontaneous Brillouin scattering (SpBS). (a) Basic configuration. LD: laser diode; PC: polarization controller; PS: polarization scrambler; PSW: polarization switcher; EDFA: erbium-doped fiber amplifier; ESA: electrical spectrum analyzer. The dashed boxes of Function Generator or Pulse generator are used for distributed SpBS measurement. (b) Three different methods to detect the weak Stokes wave, corresponding to the dotted box "i" in (a) with two optical ports (port 1 and port 2) and one electrical port (port 3).

http://dx.doi.org/10.5772/59145

The pump-probe-based experimental configuration, depicted in Fig. 6(a), is more attractive to investigate the BGS in optical fibers (especially with very short length) since SBS process occurs and high Brillouin gain can be utilized. Two light waves from a laser unit are the optical sources: the one with larger optical frequency (f_0) serves as SBS pump and the other with lower optical frequency (f_0-ν) works as SBS probe wave. They are launched into the opposite ends of FUT so as to ensure their counter-propagation and generate intense SBS interaction. The pump wave transfers intense energy to the probe wave, called Brillouin gain; in contrast, the probe wave absorbs energy from the pump wave, called Brillouin loss. The magnitude of both Brillouin gain and loss depends on the frequency offset (ν) between the pump and probe waves, determined by the Lorentzian feature of BGS (see Eq. (7)). Subsequently, the BGS can be characterized by monitoring the power of the probe wave at PD1 (i.e. Brillouin gain) [8] or that of the pump wave at PD2 (i.e. Brillouin loss) [33] as a function of ν (provided by the laser unit), respectively. Recently, a scheme based on a combination of Brillouin gain and loss was newly proposed to enhance the signal to noise ratio (SNR) of the BGS measurement [34]. It can be realized by periodic switching of the pump and probe wave and detected at either PD1 or PD2. Besides, the simultaneous detection of PD1 and PD2 followed by a subtraction may work equally.

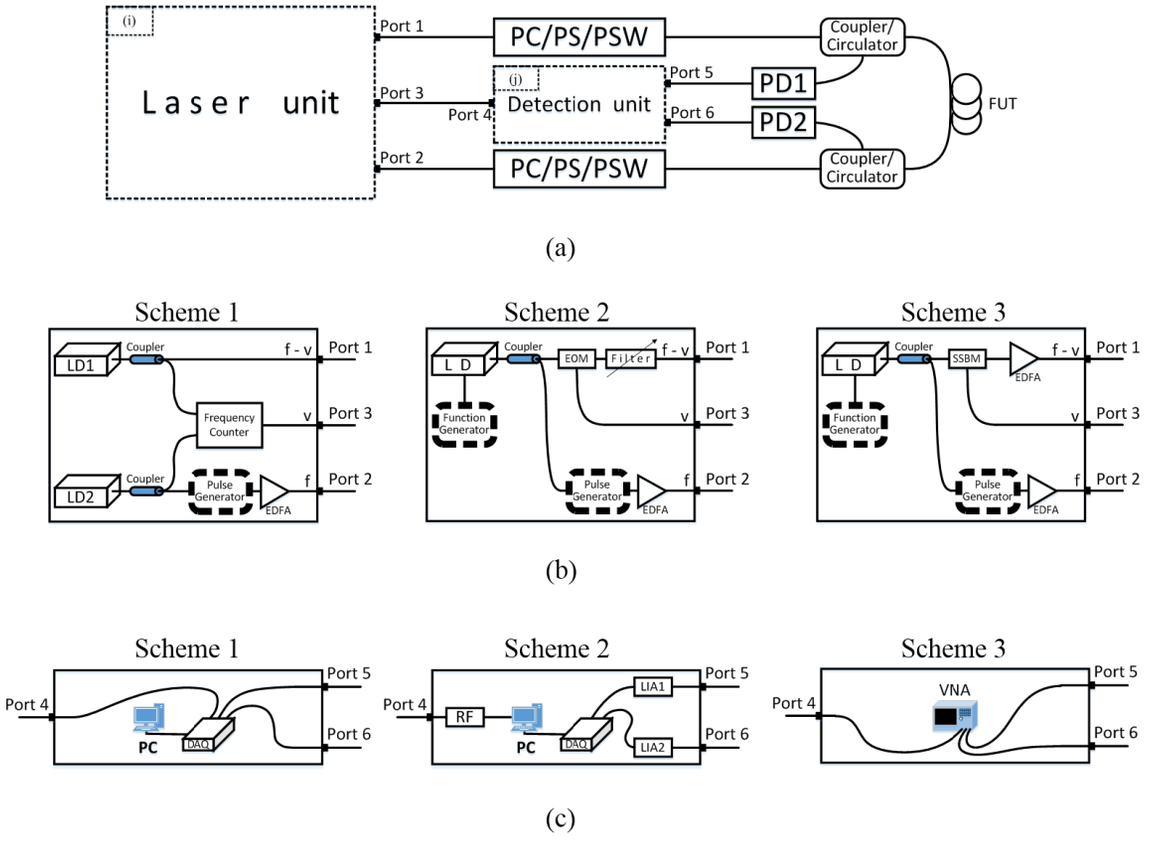

Figure 6. Experimental setup of BGS measurement based on stimulated Brillouin scattering (SBS). (a) Basic configuration. (b) Three different methods of laser unit (dotted box "i" in (a)) with two optical ports and one electrical port. The dashed boxes of Function Generator or Pulse generator are used for distributed SBS measurement. (c) Three schemes of detection unit shown in dotted box "*j*" in (a).

The laser unit shown in Fig. 6(a) comprises three ports (two corresponding to optical fields and the other to the revealed value of ν or a microwave/RF input), which has three different schemes as illustrated in Fig. 6(b). First, one can utilize two individual lasers under frequency/phase locking and frequency countering [33]. Second, one laser is divided into two parts. One part is amplified by an EDFA working as pump wave; the second part serving as probe wave is modulated by an electro-optic intensity modulator (EOM) to generate two sidebands working as probe wave[25]. An optical filter is inserted before launching into the FUT or laid after PD1 so as to cut off the influence of the frequency-upshifted sideband. Third, the second part can be also modulated by a single-sideband modulator [35] to get well-suppressed frequency-downshifted sideband directly serving as probe wave. There are also three schemes, depicted in Fig. 6(c), to realize the detection unit shown in Fig. 6(a). The first and simple scheme is related to the first scheme of the laser unit. A personal computer with a multi-channel data acquisition card (DAQ) can catch the value of ν and record the data of PD1 and/or PD2 so as to pick up the Brillouin signal (gain and/or loss) as a function of ν. The second and third schemes in Fig. 6(c) can be used for either the second and/or third laser unit in Fig. 6(b), respectively. For instance, a high-cost vector network analyzer provides a frequency-tuned RF signal to modulators and simultaneously detect the Brillouin signal [36]. Alternatively, the RF signal can be achieved from a microwave synthesizer and the data of PD1 and/or PD2 can be picked up by a DAQ with or without a lock-in amplifier (LIA). It is notable that the use of LIA for detection unit requires an intensity-chopping of the pump wave by an additional EOM [10] or periodic switching of upshifted or downshifted sideband at the SSBM [34], which is advantageous for characterization of very weak BGS or a short-length FUT due to its high SNR and accuracy[12, 34, 37].

Figure 7(a) depicts a high-accuracy experimental setup of pump-probe SBS-based BGS characterization by use of SSBM and LIA for a short-length FUT [37]. An EDFA is inserted after the SSBM to increase the probe power, which is aimed to reduce the impact of Rayleigh scattering or splicing/crack induced reflection of the pump wave in the FUT. The optical lights after a circulator include the following components:

$$P_{tot} = P_{probe}^{0} + \delta P_{probe} + P_{pump}^{R}, \tag{15}$$

where $P_{\text{probe}}{}^{0}$ denotes the probe power experiencing no Brillouin amplification, ΔP_{probe} the amplified probe power, and $P_{\text{pump}}{}^{\text{R}}$ the reflected pump power. Thanks to the lock-in detection, the component of $P_{\text{probe}}{}^{0}$ is effectively cut off by the LIA since it has no relationship with the chopped pump power given by

$$P_{pump}(t) = P_{pump}^{0} \cdot \cos(2\pi f_{ch} t), \tag{16}$$

where f_{ch} is the chopping frequency. Simply assuming that there is no depletion for pump power and no optical propagation loss for either probe or pump light, ΔP_{probe} can be expressed by

http://dx.doi.org/10.5772/59145

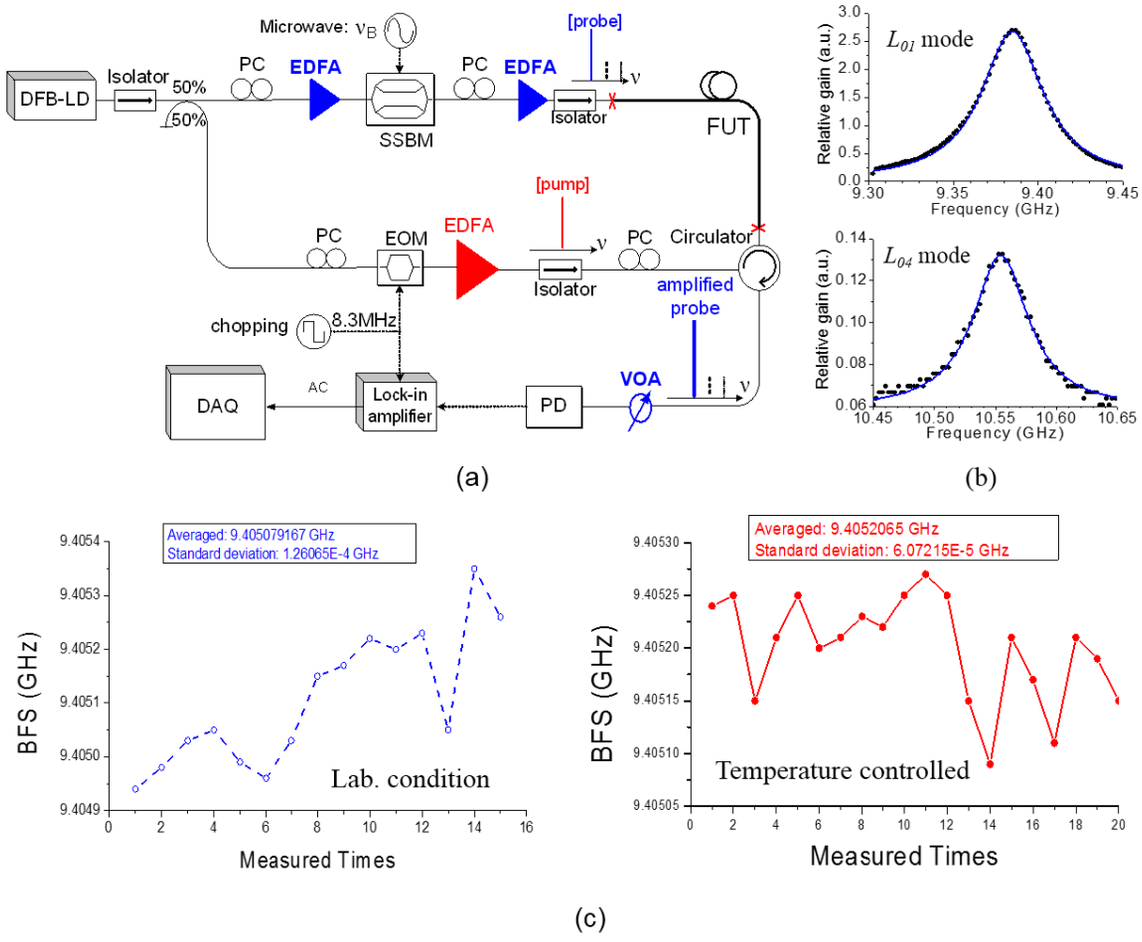

Figure 7. High accuracy pump-probe-based BGS characterization. (a) Experimental setup. (b) Characterized BGS. (c) Measurement accuracy. ((a) and (b) after Ref. [37]; © 2007 OSA.)

$$\delta P_{probe} = g(\nu) \cdot P^0_{probe}(f_0 - \nu) \cdot P_{pump}, \tag{17}$$

If R denotes the reflectivity of pump power arising from both Rayleigh scattering and some reflection points, the reflected pump power can be expressed:

$$P^R_{pump} = [P^0_{pump} - P_{loss}] \cdot R, \tag{18}$$

where P_{loss} is the so-called Brillouin loss of pump power during Brillouin interaction which is approximately equal to ΔP_{probe} as

$$P_{loss} = \delta P_{probe} = g(\nu) \cdot P^0_{probe} \cdot P^0_{pump} \cdot \cos(2\pi f_{ch} t), \tag{19}$$

The demodulated electric amplitude via a LIA at f_{ch} is given by

$$P_{de} = \left[P^0_{probe} \cdot g(\nu) \cdot (1-R) + R \right] \cdot P^0_{pump}, \tag{20}$$

where the part of $\left[P^0_{probe} \cdot g(\nu) \cdot (1-R) \right] \cdot P^0_{pump}$ is the signal to be detected by the LIA and the rest part of $R \cdot P^0_{pump}$ is the noise level. From it, one can deduce the signal-to-noise ratio (SNR):

$$SNR = \frac{P^0_{probe} \cdot g(\nu) \cdot (1-R)}{R}, \tag{21}$$

which is independent on the pump level, but just determined by the probe power of $P_{\text{probe}}{}^0$ and the reflection rate of R as well as the BGS of $g(\nu)$. In other words, an increase of probe power can drastically enhance SNR and also improve the system accuracy. As an example, Figure 7(b) shows a characterized fundamental-order or higher-order resonance BGS in a *w*-shaped high-delta fiber with fluorine inner cladding (F-HDF) [37]. The measurement system has a high accuracy of 0.13-MHz standard deviation at laboratory condition or 0.05 MHz for well-temperature-controlled condition, as illustrated in Fig. 7(c).

2.3. Pump depletion effect

As mentioned above (see Fig. 4), pump depletion effect influences the linewidth of pump-probe-based BGS. Early in 2000 [38], it was first observed that the spectrum broadening and hole burning occurs in a SBS generator (i.e. noise-started spontaneous Brillouin scattering). The reason was thought as the waveguide interaction among different angular components of the pump and backscattered Stokes signals. Besides, during the application of SBS-based amplifier, two coherent optical waves with precise frequency difference equal to Brillouin frequency shift are launched into optical fibers; then a frequency-scanned weak signal could suffer non-uniform amplification if the two waves' powers are too high [39, 40]. In SBS-based distributed fiber optical sensor, which will be introduced in **Section 3**, two coherent waves (pulse and/or continuous wave (CW)) are injected into the two opposite ends of the sensing fiber. Recently, it was found that pump depletion of pump-probe-based system configuration could induce a significant measurement error of the local Brillouin frequency shift in the far end of the probe (Stokes) wave [41].

Assuming that CW probe wave, $P_s(0)$, is injected at the near end of the fiber (z=0) while CW pump wave, $P_p(l)$, is launched at the far end of the fiber (z=l with l the fiber length). Considering the steady-state condition and neglecting the transmission loss of the fiber, the coupling equations of Eq. (4) and Eq. (5), describing the SBS interaction, can be modified to the dimensionless equations [42]:

$$\frac{dQ_p}{dx} = kQ_pQ_s, \tag{22}$$

$$\frac{dQ_s}{dx} = kQ_pQ_s, \tag{23}$$

where Q_p=P_p/P_s(0) and Q_s=P_s/P_s(0) represent the normalized pump and probe waves with respect to the injected probe wave of P_s(0), x=z/l is the normalized position, and k=G•l•P_s(0) is the normalized Brillouin gain with G=g(ν)/A_{eff}. Figure 8(a) illustrates the normalized BGS at different positions of an arbitrary-length SMF, which are numerically calculated according to Eqs. (22) and (23). It is found that BGS gradually gets broadened, saturated, and hole-burned when the position moves from the far end (z=l) towards the near end of the fiber (z=0). We define the BGS saturation as the critical condition of spectral hole burning phenomenon.

Further introduce the injected power ratio between pump and probe waves, defined as γ=Q_p(x=1)=P_p(l)/P_s(0). Since dQ_p/dx=dQ_s/dx, the difference between Q_p and Q_s maintains a constant (A), i.e. A=Q_p-Q_s, which is determined by k and γ. Consequently, the analytical solutions to Eqs. (22) and (23) are derived as

$$Q_p = \frac{A(A+1)e^{-kAx}}{(A+1)e^{-kAx}-1}, \tag{24}$$

$$Q_s = \frac{A}{(A+1)e^{-kAx}-1}. \tag{25}$$

The critical condition of the spectral hole burning phenomenon can be theoretically expressed by:

$$\frac{dQ_s}{d\nu} = 0. \tag{26}$$

By numerically solving Eqs. (24)-(26), one can interpret the critical condition by two different ways: (1) the critical position x_c for the fixed pump and probe power; (2) the critical powers for a specific position of the fiber. Figure 8(b) depicts the calculated relation of x_c to k and γ, which indicates that x_c moves towards the fiber far end when k and γ reach higher values (i.e. the fiber gets longer or the injected powers are stronger). It means that the pump depletion gets worse since much longer segments in the fiber suffer spectral hole burning. It is notable to address that the physical nature of the critical powers is essentially the same as that of the critical position because they can be also deduced by the contour (i.e. k-γ curve) at a fixed position x in Fig. 8(b):

$$P_s(0) = k / GL, \tag{27}$$

$$P_p(L) = \gamma k / GL. \tag{28}$$

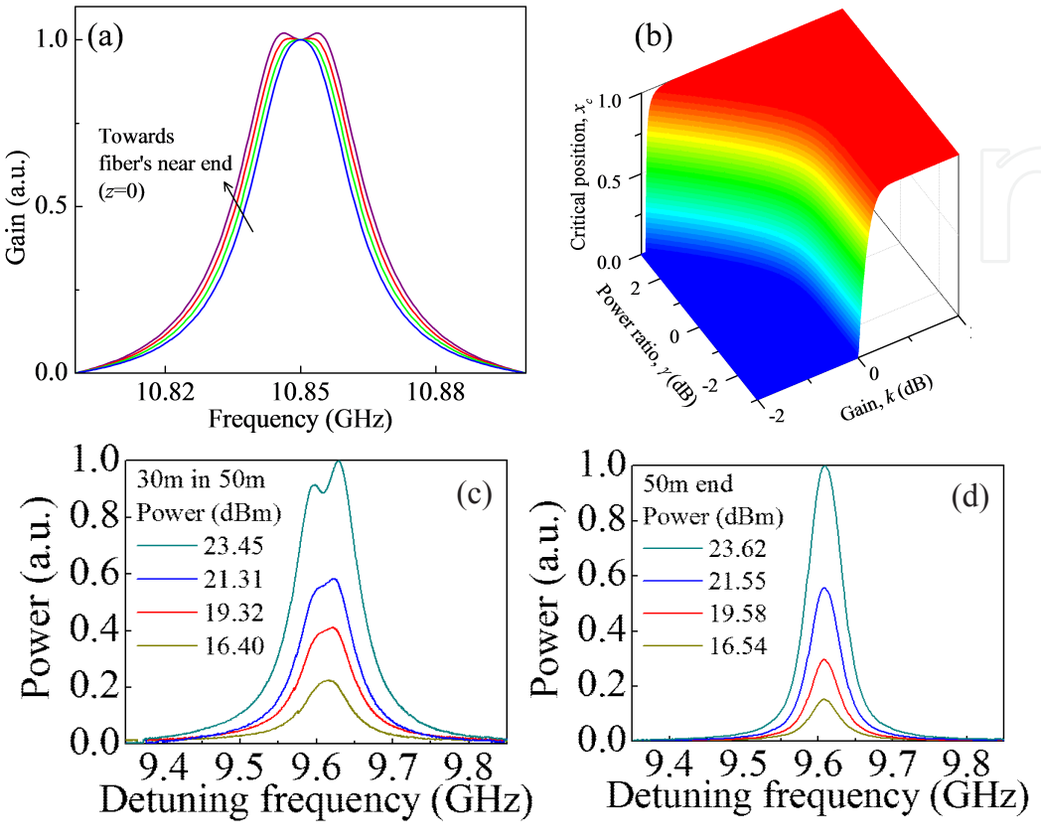

Figure 8. (a) Simulated BGS at different positions in the fiber. (b) Critical position x_c, determined by the normalized gain k and injected power ratio γ. The critical positions divide the fiber into two parts with and without the spectral hole burning phenomenon. Measured BGS in the middle (c) or at the end (d) of a 50-m-long fiber. (after Ref. [42]; © 2014 JJAP.)

Figure 8(c) and 8(d) illustrates the measured BGS under different pump power for two different positions (in the middle and at the far end, respectively) of a 50-m-long dispersion compensated fiber (DCF). The probe power is fixed at 9.8 dBm. At the far end, the BGS [see Fig. 8(d)] rises with the power increased but always preserves the Lorentz shape. While in the middle, the experimental result [see Fig. 8(c)] is in a qualitative accordance with the numerical analysis [see Fig. 8(a)]. The Brillouin gain keeps rising with the increase of optical power, while the peak at the local Brillouin frequency shift seems to be saturated gradually and a hollow starts appearing when it reaches ~20 dBm, which is just the spectral hole burning phenomenon. The hollow in the BGS may introduce great errors to pump-probe-based Brillouin distributed sensors since it disables the peak-searching of the Brillouin frequency shift.

The pump power leading to the BGS saturation is approximately characterized as the critical pump power (for instance, 21.3 dBm at z=30 m). The measured critical powers for two positions (z=20 m or 30 m) of 50-m-long DCF are depicted in Fig. 9, where the simulated critical powers are compared. It illustrates that the critical pump powers approximately measured for several

probe powers (open symbols) have very similar trend as the theoretical analysis (curves). It is clear that the position of bigger z requires greater critical powers. This is because the pump depletion is weaker and the distortion of the BGS is less serious if the position is much closer to the fiber far end.

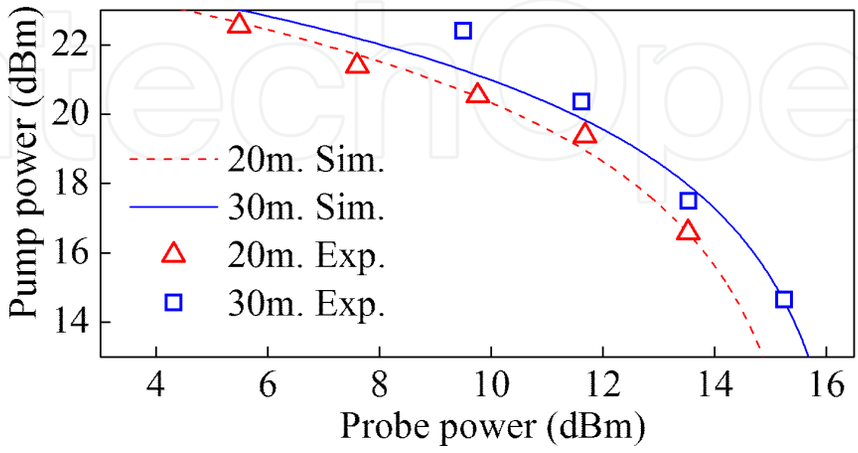

Figure 9. Critical powers for two different positions in a 50-m-long DCF. Solid and dashed curves, simulation; open symbols: experiment. (after Ref. [42]; © 2014 JJAP.)

3. Brillouin–based distributed sensors

3.1. Sensing of measurands

The first report of Brillouin based distributed optical fiber sensors [43] was based on the same principle as that of optical time domain reflectometry (OTDR) or Raman based OTDR (ROTDR) technique as a non-destructive attenuation measurement technique for optical fibers. In that proposal [33], SBS process was performed by injecting an optical pulse source and a continuous-wave (CW) light into two ends of FUT. When the frequency difference of the pulse pump and CW probe is tuned offset around ν_B of the FUT, the CW probe power experiences Brillouin gain from the pulse light through SBS process. Similarly like the case of OTDR, the SBS distributed measurement could measure attenuation distribution along the fiber having no break from an interrogated optical power as a function of time, but it has much higher signal-to-noise ratio (more than ~10 dB) than OTDR due to SBS high gain. Later, Horiguchi and co-researchers found that this non-destructive can be extended into **a frequency-resolved technique** because ν_B of optical fibers has linear dependence on measurands of strain and temperature as follows [44, 45]:

$$\nu_B - \nu_{B0} = A \cdot \delta\varepsilon + B \cdot \delta T, \tag{29}$$

where ν_{B0} is measured at room temperature (25°C) and in the "loose state" as a reference point, $\Delta\varepsilon$ the applied strain and ΔT the temperature change. The "loose state" means that the FUT is laid freely in order to avoid any artificial disturbances. A *(or* $C\nu\varepsilon$) is the strain coefficient in a unit of MHz/$\mu\varepsilon$ and B *(or* $C_T\varepsilon$) is the temperature coefficient in a unit of MHz/°C. Figure 10 illustrates the characterized strain or temperature dependence in a standard SMF under the experimental setup of Fig. 7(a), where the BGS always moves towards higher ν_B and its gain reduces or increases when $\Delta\varepsilon$ or ΔT is increased, respectively. At 1550 nm, A=0.04~0.05 MHz/$\mu\varepsilon$ and B=1.0~1.2 MHz/°C, which depends on the fiber's structure and jackets**. Note that Eq. (29) is the basic sensing mechanism of Brillouin-based distributed sensors.**

The nowadays telecom optical fibers (ITU-T G.651, G.652, G.653, and G.655) mostly have GeO_2-doped fiber cores [46] and pure-silica (or other-doped-silica) cladding. Naturally, the GeO_2 doping induces the reduction of the longitudinal acoustic velocity in GeO_2-doped core V_{l1} with respect to that in pure-silica cladding V_{l2} (i.e. $V_{l1} < V_{l2}$) [24, 47]. It provides a waveguide of longitudinal acoustic modes in the core region as schematically depicted in Fig. 3(b). A recent study further proves that the acoustic modes sense better confinement than the optical modes in a GeO_2-doped optical fiber [13]. The enhanced confinement results in the existence of multiple L_{0l} acoustic modes in a single-mode optical fiber (SMF) [8], and also leads to that the first-order L_{01} acoustic mode among all L_{0l} modes is best confined in the core and even better confined than the fundamental LP_{01} optical mode [13]. Furthermore, the enhanced confinement shows that the effective acoustic velocity of L_{01} mode (V_a) is close to V_{l1} (i.e. $V_a \approx V_{l1}$), the longitudinal acoustic velocity in the core. Therefore, the change of the L_{01} mode's effective acoustic velocity V_a is dominantly due to the change of the core's acoustic velocity V_{l1} but negligibly (less than 1%) due to that of the cladding's acoustic velocity V_{l2}, even though the core's acoustic velocity V_{l1} and the cladding's acoustic velocity V_{l2} vary equally [12].

The longitudinal acoustic velocity V_{l1} in the GeO_2-doped core (approximately, the L_{01} mode's effective acoustic velocity V_a) is determined by the Young's modulus (E_1) and the density (ρ_1) [48]:

$$V_a \approx V_{l1} = \sqrt{E_1 / \rho_1}, \tag{30}$$

For convenience, we introduce a normalized strain coefficient ($A'=A/\nu_{B0}$, in a unit of $10^{-6}/\mu\varepsilon$) and a normalized temperature coefficient ($B'=B/\nu_{B0}$, in a unit of 10^{-6}/°C). The normalized strain coefficients include three respective factors[49]:

$$A' \equiv \frac{A}{\nu_{B0}} = A'_{neff} + A'_{\rho} + A'_{E}, \tag{31}$$

$$B' \equiv \frac{B}{\nu_{B0}} = B'_{neff} + B'_{\rho} + B'_{E}. \tag{32}$$

http://dx.doi.org/10.5772/59145

Each three parts in the right sides of Eq. (31) and Eq. (32) are determined by relative change rates in n_{eff}, E_1, and ϱ_1 due to the applied strain $\Delta\varepsilon$ or the temperature change ΔT. A'_{neff} and B'_{neff} are determined by the elasto-optic and thermo-optic effects; A'_{ρ} and B'_{ρ} are subject to the strain-induced distortion and the thermal expansion; A'_{E} and B'_{E} are decided by the strain-induced second-order nonlinearity of Young's modulus and the thermal-induced second-order nonlinearity of Young's modulus.

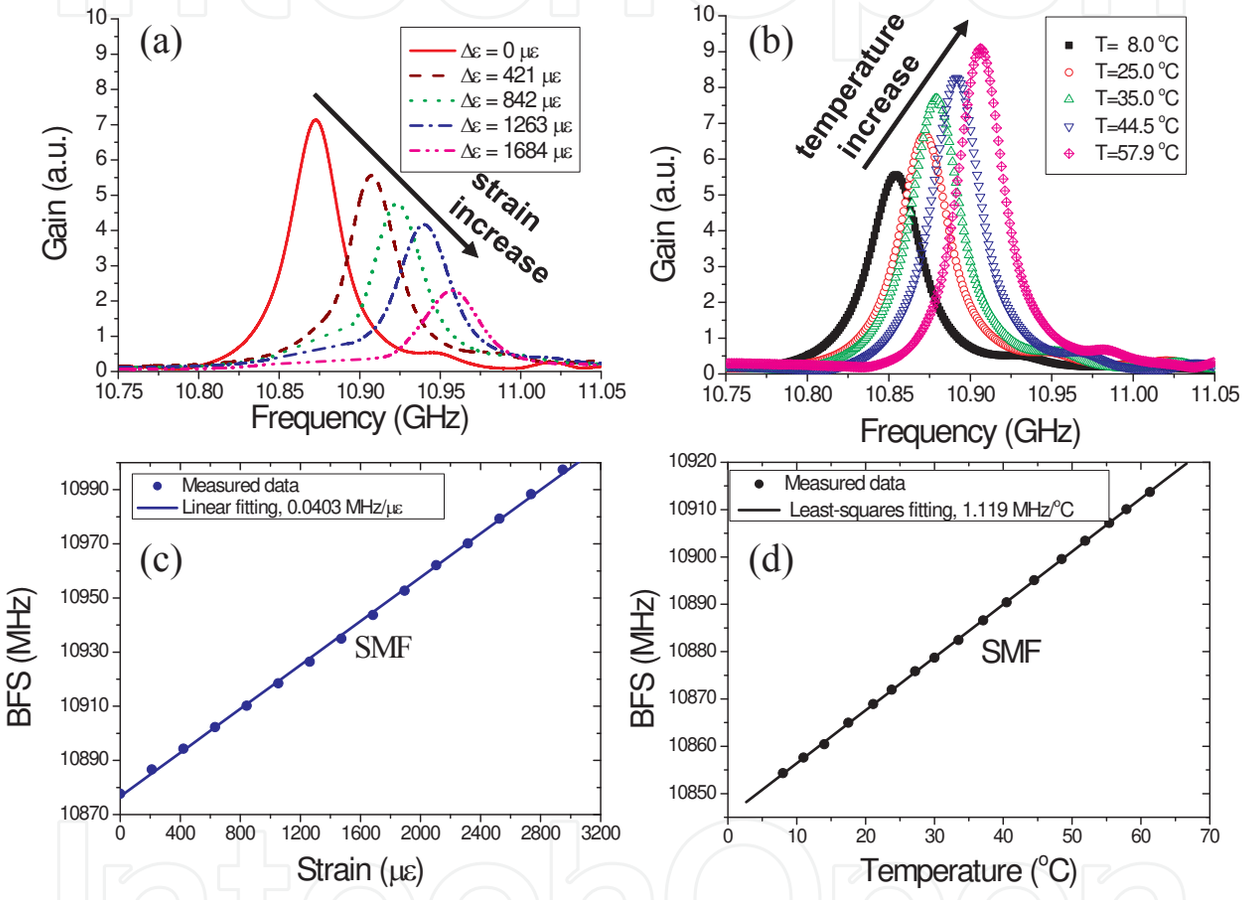

Figure 10. (a) Stain and (b) temperature dependences of BGS in SMF; (c) Strain and (d) temperature dependences of Brillouin frequency shift ν_B in SMF.

Strict experimental characterization on a series of optical fibers with different GeO_2 concentration is depicted in Fig. 11 [49]. The BFS has linear dependence on the GeO_2 concentration in the fiber's core (i.e.-87.3 MHz/mol%), which corresponds to ν_{B0} change of-87.3 MHz regarding 1-mol% increase of GeO_2 concentration in the core (i.e. an incremental Δ of 0.1 %). It specifies the previously reported values [25, 50, 51]. Besides, the frequency spacing between neighbouring acoustic modes increases by orders when the GeO_2 concentration is enhanced, for example, ~50-60 MHz for Fiber-A (SMF, 3.65 mol%) versus ~700-720 MHz for Fiber-C (HNF, 17.0 mol%).

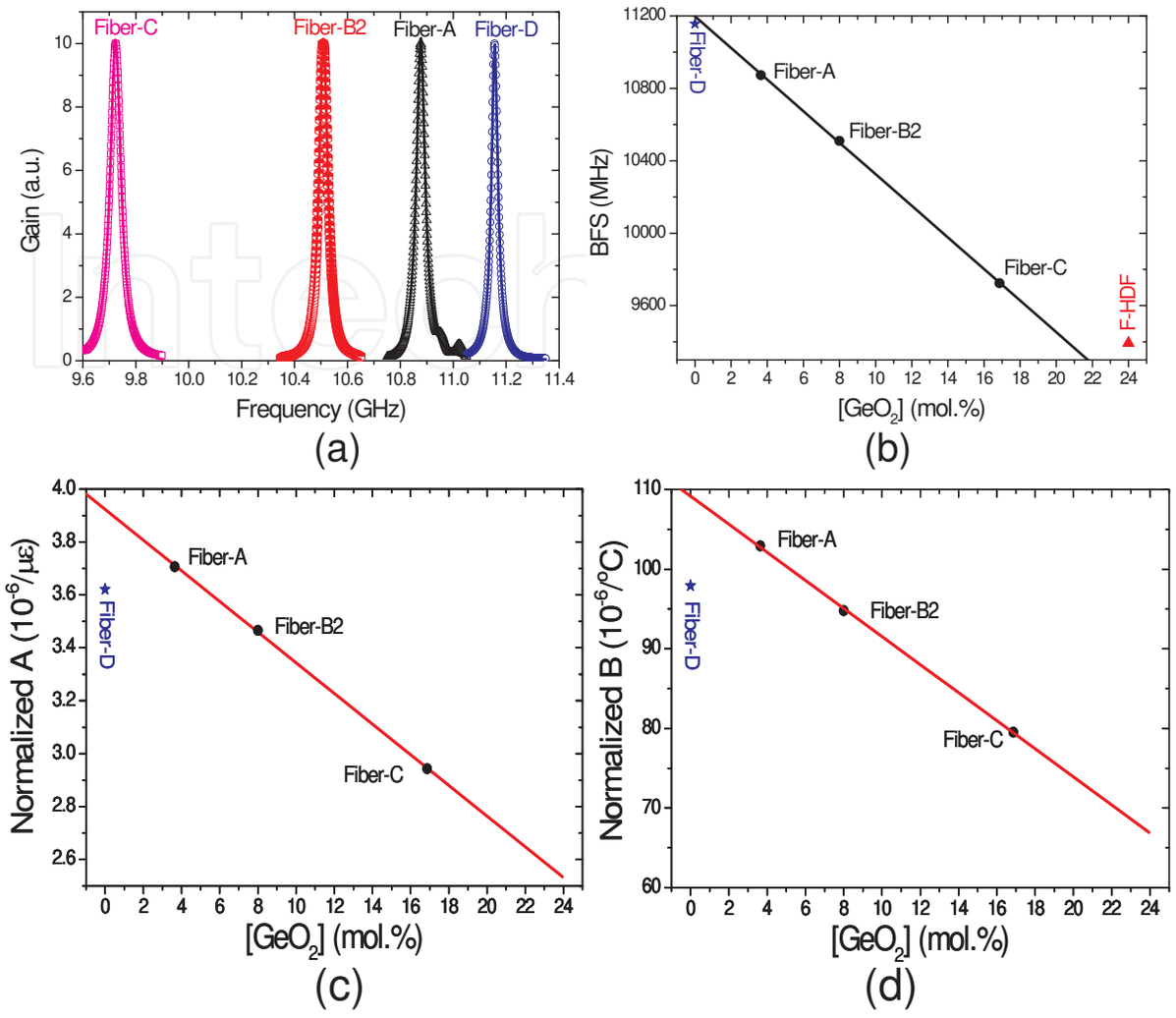

Figure 11. (a) BGS, (b) BFS, (c) normalized strain coefficient, and (d) normalized temperature coefficients in silica optical fibers with different GeO_2 concentration. (After Ref. [49]. © 2008 OSA/IEEE.)

The normalized strain and temperature coefficients defined in Eq. (31) and Eq. (32) were characterized by repeating the BGS measurement under different applied strain and temperature change. It shows a linear dependence of A' or B' on GeO_2 concentration with slope of-1.48 %/mol% or-1.61 %/mol%, which denote that A' and B' are relatively decreased by-1.48 % and-1.61 % for an incremental Δ of 0.1 %. The theoretical study further indicates that both the strain and temperature dependences in Eq. (29) are dominantly (~92%) responsible from the strain-induced and thermal-induced second-order nonlinearities of Young's modulus, that is, Eq. (31) and Eq. (32) [49].

3.2. Sensing of location

Besides the sensing of measurands (see Eq. (29)), the mapping of spontaneous or stimulated Brillouin scattering process (not just non-destructive attenuation measurement [43]) is another

key issue to realize distributed optical fiber sensing [52-54]. Two different mapping ways, as schematically illustrated in Fig. 12, were proposed. One is to repeat the localized BGS in scanned positions along the FUT; the other is to repeat the Brillouin interaction under different frequency offset.

There are three different mapping or position-interrogation techniques, including time domain [33, 52-56], frequency domain [57, 58], and correlation domain [59-61]. Regarding the injection ways of optical fields, there are two opposite groups, i.e. analysis versus reflectometry. The analysis is two-end injection based on SBS; while the reflectometry is one-end injection based on SpBS. Comparably, the analysis has much higher SNR than the reflectometry. Note that there is an additional method between analysis and reflectometry, called one-end analysis [55, 62, 63]. Its only difference from the traditional (two-end) analysis is the one-end injection and its SBS process occurs between the forward pump and the backward probe wave that is reflected at the far end of FUT.

The basic principle of time-domain sensing technique is the "time-of-flight" phenomenon in FUT. For two-end or one-end analysis, named Brillouin optical time domain analysis (BOTDA) [33, 52, 54], one of pump and probe waves is pulsed in time and the other is continuous wave (CW). Subsequently, they are successively interacted along the FUT during the time-of-flight of the pulsed wave. In contrast, for one-end reflecometry, called Brillouin optical time domain reflectometry (BOTDR) [53, 56], the pump wave is pulsed in time and the SpBS Stokes wave is reflected along the FUT during the pump's time-of-flight. The basic experimental configuration of BOTDR or BOTDA can be simply carried out in Fig. 5 or Fig. 6, respectively. The required modification is to insert an optical pulse generator (for example, an electro-optic intensity modulator driven by an electric pulse generator). The spatial resolution (ΔZ_{TD}) of time-domain distributed sensing is physically determined by the pulse width (τ)[43]:

$$\Delta Z_{TD} = \frac{\tau \cdot c}{2n}, \tag{33}$$

where c is the light speed in vacuum and n the group velocity of the pulse. The BGS mapping is realized by repeating the above measurement when the spectrum of the reflected Stokes in BOTDR is processed or the optical frequency offset between the pump and probe in BOTDA is tuned around the BFS ν_B.

There are two kinds of correlation-domain sensing techniques, nominated Brillouin optical correlation domain analysis (BOCDA) [59, 60] and Brillouion optical correlation domain reflectometry (BOCDR) [61, 64]. Both of them originate from the so-called synthesis of optical coherence function (SOCF) [65, 66]. Nevertheless, the SOCF in BOCDA or BOCDR is generated between the pump and probe waves or between the pump-scattered Stokes wave and the optical oscillator, respectively. In experiment, the BOCDR and BOCDA can be executed by substituting a distributed feedback laser diode (DFB-LD) driven by a function generator (such as in a sinusoidal function) for the light source in Fig. 5 and Fig. 6, respectively. Thanks to the current-frequency transferring effect of DFB-LD [67], the optical frequencies of the light

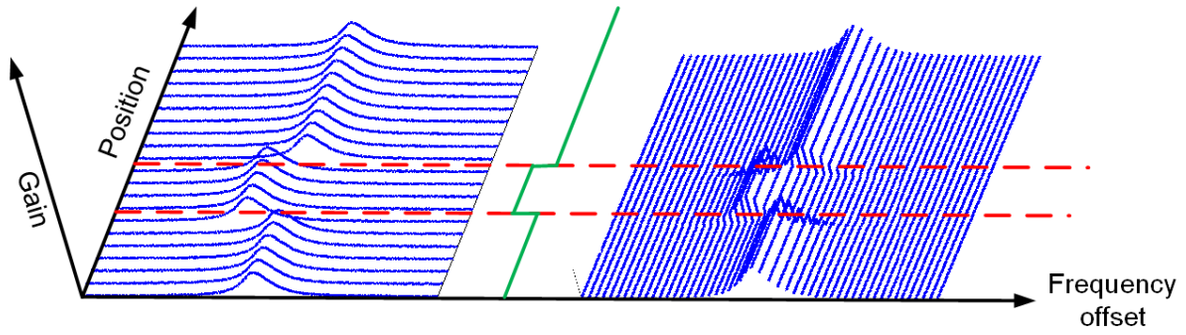

Figure 12. Schematic of sensing of location or mapping of BGS.

sources are simultaneously modulated also in a sinusoidal function. Subsequently, the optical frequency offset between pump and probe or between scattered Stokes and optical oscillator changes with time as well as position, deviating from the preset constant frequency offset around the BFS ν_B. Only at some particular locations (called correlation peaks), the frequency offset is maintained as the constant frequency offset because of the in-phase condition so that the local SBS interaction or the beating of the local Stokes and oscillator is **constructive**. At other locations rather than correlation peaks, the frequency offset is always vibrating with time, which leads to a broadened and **destructive** SBS or SpBS. The spatial resolution of BOCDA and BOCDR are both determined by[59]

$$\Delta Z_{CD} = \frac{c}{2nf_m} \cdot \frac{\Delta \nu_B}{\pi \Delta f}, \tag{34}$$

where f_m is the modulation frequency of the sinusoidal function, Δf the modulation depth, and $\Delta\nu_B$ the Brillouin linewidth defined in Eq. (10). Since the SOCF is naturally realized by an integral or summation signal processing in photonics or electronics, all SBS or SpBS along the entire FUT should be accumulated together (as an example shown in Fig. 6(a), accumulated by a LIA). Consequently, the maximum measurement length (or sensing range, L_{CD}) is decided by the distance between two neighboring correlation peaks [59]:

$$L_{CD} = \frac{c}{2nf_m}. \tag{35}$$

Because of the difference of the physical pictures between time domain and correlation domain, their sensing performance is different. For example, the spatial resolution of BOTDA/BOTDR was typically limited to be ~1 m by the lifetime of acoustic phonons (10 ns) and the nature of intrinsic Brillouin linewidth. However, BOCDA/BOCDR is of CW nature free from this limitation, and their spatial resolution can be ~cm-order [60, 68] or even ~mm-order [69]. Since BOTDA/BOTDR carries out the whole mapping of BGS along the FUT during the time-

of-the-flight while BOCDA/BOCDR realizes the distributed sensing by sweeping the modulation frequency (or correlation peak), the sensing speed is different. The entire sensing speeds for both BOTDA/BOTDR and BOCDA/BOCDR are time-consuming due to the tuning of pump-probe frequency offset, averaging of mapping, and signal processing of data fitting. However, the sensing position of BOCDA/BOCDR can be random accessed [59, 61], and the dynamic sensing with high speed at the random accessed position is possible [70, 71]. The detailed difference of other performances will be described in **Section 4** and **Section 5**.

4. Challenges in Brillouin based distributed optical fiber sensors

4.1. Simultaneous measurement of strain and temperature

As explained in **Section 3**, all Brillouin based distributed optical fiber sensors interrogate the Brillouin frequency shift so as to deduce strain and temperature information based on Eq. (29). It naturally gives a physical challenge, i.e. how to distinguish the response of strain from the response of temperature based on the single parameter of BFS interrogation in a single piece of sensing fiber. In current industrial practices, two individual fibers or two fibers in a fiber cable are used to discriminate the strain and the temperature: the first one is embedded or bonded at the target material/structure to feel the total responses of strain and temperature, while the second fiber is placed beside the first one and kept in loose condition so that it feels the response of temperature only. Another way is to use two distributed sensing systems with two individual fibers [72-75]: one Raman-based or Rayleigh-based sensor is to monitor the temperature; the other Brillouin sensor to monitor the temperature and strain. After distributed sensing measurements, the strain and temperature responses can be calculated by mathematics. However, the above practices make the entire sensing system complicated and the calculated responses of strain and temperate change with service time.

Practical applications of Brillouin based distributed optical fiber sensors require a method to effectively discriminate them by use of two intrinsic parameters (denoted by y_1 and y_2) in one sensing fiber. Their changes (Δy_1 and Δy_2) depend on simultaneously the applied strain ($\Delta\varepsilon$) and temperature change (ΔT), which are governed by the following matrix:

$$\begin{pmatrix} \Delta y_1 \\ \Delta y_2 \end{pmatrix} = \begin{pmatrix} A_1 & B_1 \\ A_2 & B_2 \end{pmatrix} \begin{pmatrix} \Delta\varepsilon \\ \Delta T \end{pmatrix}, \tag{36}$$

where A_1 (A_2) and B_1 (B_2) are the strain and temperature coefficients of y_1 (y_2), respectively. Both $\Delta\varepsilon$ and ΔT can be deduced from Eq. (36), given by

$$\begin{pmatrix} \Delta\varepsilon \\ \Delta T \end{pmatrix} = \frac{1}{A_1 B_2 - B_1 A_2} \begin{pmatrix} B_2 & -B_1 \\ -A_2 & A_1 \end{pmatrix} \begin{pmatrix} \Delta y_1 \\ \Delta y_2 \end{pmatrix}, \tag{37}$$

It is obvious to know that the condition that the strain and temperature can be successfully distinguished is determined by

$$A_1 B_2 \neq B_1 A_2. \tag{38}$$

In fact, the Brillouin-based distributed sensing system always suffer a measurement uncertainty (Δy_1 and Δy_2), which is in a linear proportional relation with the discrimination errors in strain ($\Delta\varepsilon$) and temperature (ΔT), also given by Eq. (37).

A possible solution using one fiber is to monitor two acoustic resonance peaks at different orders of Brillouin gain spectrum (BGS) in a specially-designed optical fiber [13, 37, 76, 77]. So far, this method cannot ensure accurate discrimination because all the acoustic resonance frequencies exhibit similar behaviors in their dependences on strain and temperature (see Fig. 11) [49]. There is another kind of method reported for discrimination that relies on the possibility that the peak amplitude and BFS of the BGS could have quantitatively different dependences on strain and temperature [78-81]. Its accuracies is not sufficient (e.g., several degrees Celsius and hundreds of micro-strains), which is mainly due to the low signal-to-noise ratio in the BGS peak-amplitude measurement particularly for distributed sensing where troublesome noise from non-sensing locations is accumulated.

4.2. System limitation of time-domain or correlation-domain technique

There are several system limitations in time-domain BOTDA/BOTDR and correlation-domain BOCDA/BOCDR, which comes from their individual sensing techniques. For example, BOTDA/BOTDR suffers a typical limitation of spatial resolution (~1 m) mainly determined by the linewidth of BGS or the lifetime (~10 ns) of acoustic phonons. Narrower pulse width corresponding to higher spatial resolution according to Eq. (33) weakens the acoustic phonons due to the lifetime of the acoustic phonons and leads to broader BGS as well as lower frequency accuracy due to the convolution between the intrinsic BGS and broader spectrum of the pulse [82, 83]. Moreover, although the time-of-the-flight feature of BOTDA/BOTDR is suitable for long distance sensing, the nature of pump depletion and fiber transmission loss confines the maximum of measurement range within several tens of kilometers [84].

On the other hand, BOCDA/BOCDR can provide extremely high spatial resolution of cm order or mm order with a cost of system complexity. However the correlation-domain sensing nature means that there intrinsically exist periodic correlation peaks in the fiber. Besides, the nominal definitions of spatial resolution and measurement range (see Eq. (34) and Eq. (35)) show that they both depend on the modulation frequency and thus they are in a tradeoff relation with each other [59]. The accumulation of the entire BGS along the FUT corresponding to the measured BGS at the sensing location should include a high-magnitude background of the BGS at the uncorrelated positions, which makes it difficult achieve large range of strain or temperature since higher strain or temperature change shifts the measured BGS closer to the background. As introduced in **Section 3.2**, the access ability of BOCDA/BOCDR is random and the sensing speed in one location is high. However, the

sensing speed along the entire FUT is still low and just comparable to BOTDA/BOTDR because the scanning of the sensing location is realized by changing the modulation frequency (see Eq. (35)), which needs quite long time to restart the communication among electronic devices (specially, function generator).

5. Advances in Brillouin based distributed optical fiber sensors

5.1. Concept of Brillouin dynamic grating

Dynamic grating can be generated by use of gain saturation effect in rare-earth-metal-doped optical fibers [85-87] or stimulated Brillouin scattering (SBS) process in optical fibers [88-93] and even in a photonic chip [94]. Dynamic grating is more advantageous for certain applications than fiber Bragg grating (FBG) [95] because it can be dynamically constructed using two coherent pump waves while FBG is static after fabrication. In comparison, the SBS-generated dynamic grating, also called Brillouin dynamic grating (BDG), is superior to the saturation gain grating due to its elasto-optic nature and lack of quantum noise [1]. In addition, the BDG is much easier to experimentally characterize [88, 90-93] while the saturation gain grating needs sophisticated double lock-in detection [86].

Up to date, there are various methods to generate BDG in optical fibers, which are schematically compared in Fig. 13 [93]. The basic principle of BDG in optical fibers is quite similar, which is shown in Fig. 13(a). Two coherent optical waves, i.e. the pump and probe (or Stokes) waves in the SBS process, are launched from the two opposite ends of optical fibers. When their optical frequency offset ($\nu_1 = f_1 - f_1'$) is equal to the BFS ν_B as well as the resonance frequency of the fundamental acoustic mode ($\nu_{ac}^{(1)}$) defined by Eq. (8):

$$\nu_1 \equiv f_1 - f_1' = \nu_B = \nu_{ac}^{(1)}, \tag{39}$$

where f_1 and f_1' are the optical frequencies of the pump and probe waves, a strong acoustic wave of the fundamental acoustic mode (the so-called BDG) is optically generated. As long as the third optical wave (i.e. the readout wave) is injected from the same end as the pump wave, there is a diffracted/reflected optical wave originating from the BDG. The diffraction or reflection efficiency (also called BDG reflectivity) is determined by the phase-matching condition, under which the pump/probe and readout wave can efficiently couple their energy via the BDG.

The method of BDG generation and detection can be classified into two different cases, which depends on the used optical fibers. In the first case of polarization maintaining fiber (PMF) [88-90] or few-mode fiber (FMF) [91] (see Fig. 13(b)), the BDG generation is separated from the BDG detection by use of orthogonal polarization states or different optical modes, respectively. The phase-matching condition means that the BFS of the BDG generation and detection should be unique as Eq. (39), which results in a frequency difference determined by the PMF's

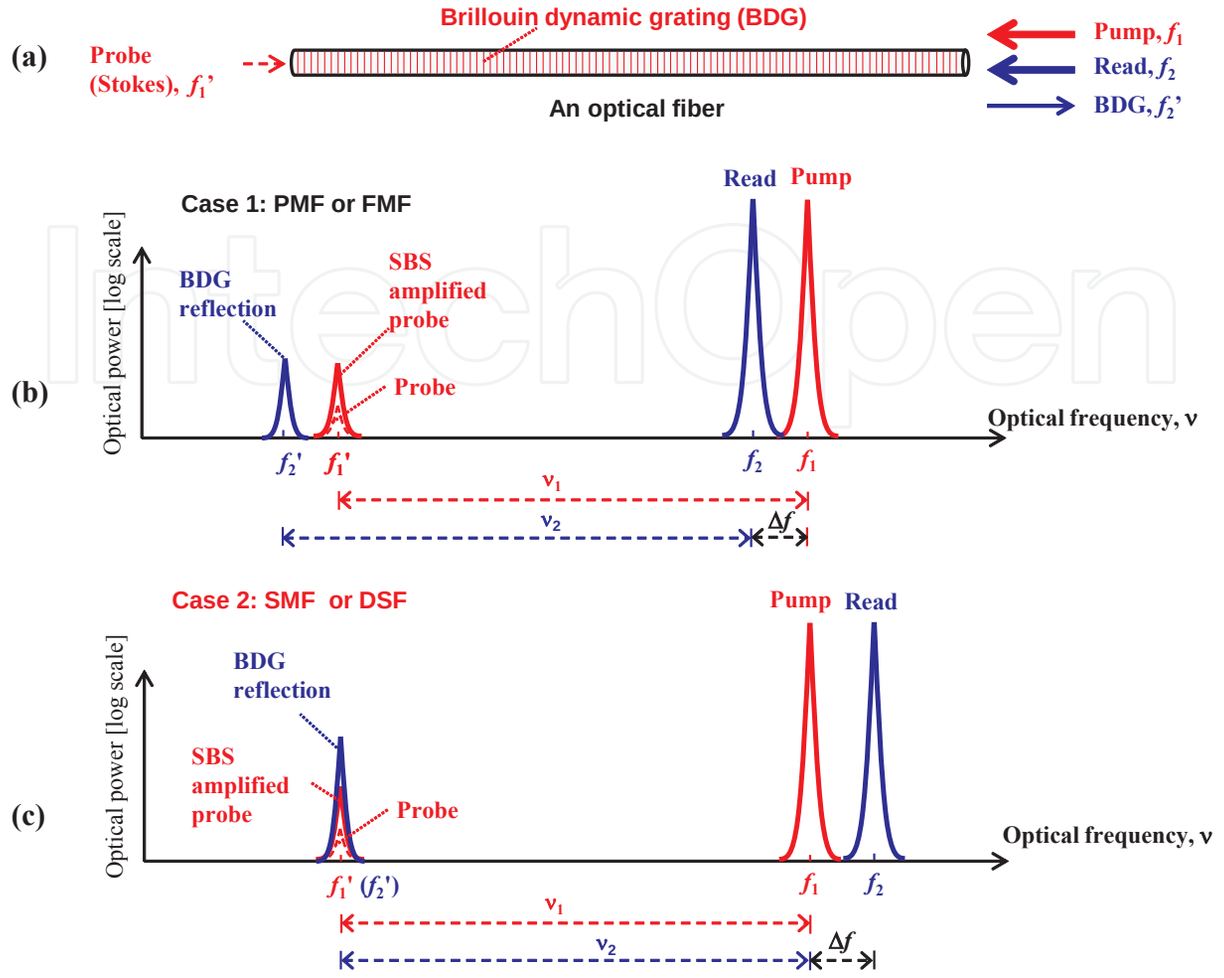

Figure 13. Principle of BDG in an optical fiber. (a): Orientation of optical injection. (b) and (c): Two different cases of the optical frequency relation among the pump, probe (Stokes), readout, and BDG reflection. (After Ref. [93]; © 2013 OSA.)

birefringence (B) or the FMF's modal refractive index difference (n_{eff}-n_{eff}' with n_{eff}' the higher-order modal refractive index):

$$\Delta f \equiv f_2 - f_1 = \frac{B}{n_{eff}} \cdot f_1, \tag{40}$$

$$\Delta f \equiv f_2 - f_1 = \frac{n_{eff} - n_{eff}'}{n_{eff}} \cdot f_1, \tag{41}$$

where f_2 is the optical frequency of the readout wave.

As shown in Fig. 13 (c), the BDG in a SMF [92] or dispersion shifted fiber (DSF) [93] can be generalized into the second case. If the readout wave with the optical frequency of f_2 is

launched for BDG detection, multiple-peak Stokes wave is intrinsically backscattered via SpBS. The *i*th-peak Stokes wave is downshifted in frequency from the readout wave by

$$\nu_2^{(i)} = \frac{2n_{eff}}{c} \cdot V_a^{(i)} \cdot f_2, \tag{42}$$

where $V_a^{(j)}$ is the acoustic velocity of the *i*th-order acoustic wave. The phase-matching condition of the BDG generation and detection turns to be determined by the frequency difference between the pump and readout wave:

$$\Delta f \equiv f_2 - f_1 = \frac{\nu_1^{(i)} - \nu_1^{(1)}}{1 - 2n \cdot V_a^{(i)} / c} \approx \nu_1^{(i)} - \nu_1^{(1)}, \tag{43}$$

where $\nu_1^{(j)}$ is the *i*th-order resonance frequency of the BGS measured by the pump-probe SBS process, also given by Eq. (42) except that f_2 is replaced by f_1. The approximation in Eq. (43) is reasonable since the acoustic velocity ($V_a^{(j)}$=~5300-5900 m/s) in silica-based fibers is far smaller than the optical velocity (c=3.0× 10^8 m/s) [11]. Note that the BDG observed in a SMF [92] can be regarded as one special example of the generalized second case with$\Delta f = 0$ or $f_2 = f_1$ in Eq. (43) because the BDG generation and detection share the same fundamental acoustic mode.

In comparison, the method based on a PMF is more attractive because the BDG generation and readout are oriented and separated in two orthogonal polarization states [88-90]. The frequency-deviation property provides an additional degree of freedom to precisely characterize the birefringence according to Eq. (28). Figure 14 depicts the optical spectra of the BDG reflection measured by an optical spectrum analyzer (OSA), including four components (leaked pump and probe waves, BDG reflected wave, and Rayleigh scattered wave from left to right). The BDG property is qualitatively confirmed by the great enhancement of the third component (BDG reflected wave), since it is transferred from weak SpBS to strong SBS process under the assistance of the BDG generated by pump and probe waves. The frequency deviation can be roughly estimated to be 44.0 GHz by a wavelength meter, which gives the birefringence value of 3.28*10^{-4}. However, the resolution is limited to about 1*10^{-6} due to 0.1 GHz-level resolution of the wavelength meter.

Most recently, a heterodyne detection was demonstrated to straightforwardly characterize the physical BDG property in a high-delta PMF [96]. Figure 15(a) summarizes a 3D distribution of the heterodyne-detected electronic spectra between the BDG reflection and the readout wave while scanning the pump–probe frequency offset (ν_1 or f_1-f_1') around the BFS of 10.510 GHz. The peak frequency and power dependence of the on f_1-f_1' are shown in Fig. 15(b) and Fig. 15(c), respectively. The frequency dependence is a linear relation because the acoustic resonance frequency of the BDG is determined by f_1-f_1' so that the diffraction wave suffers the identical frequency downshift from the readout wave. The Brillouin gain determined by the

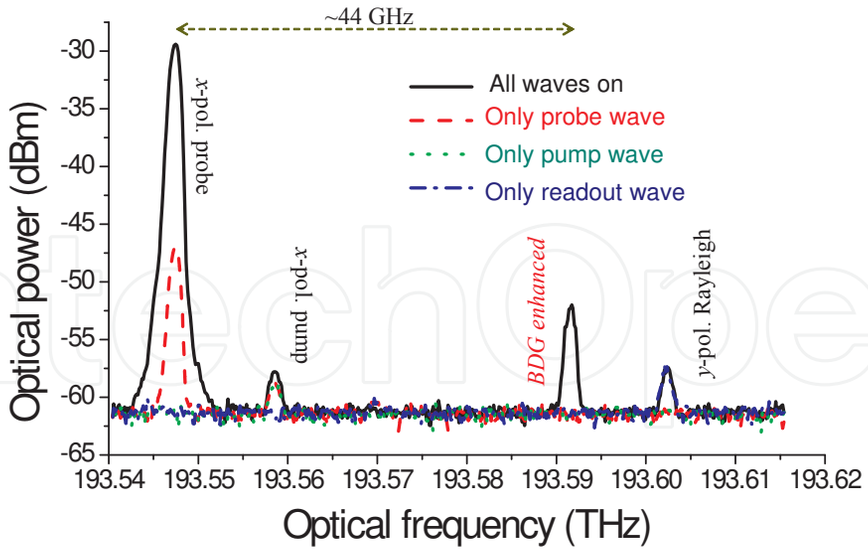

Figure 14. Qualitative characterization (optical spectra) of BDG reflection in a PMF with B=3.3*10^{-4}. Black-solid, all pump, probe and readout waves are launched; blue-dash-dotted, only readout wave; red-dashed, only probe wave; green-dotted, only pump wave.

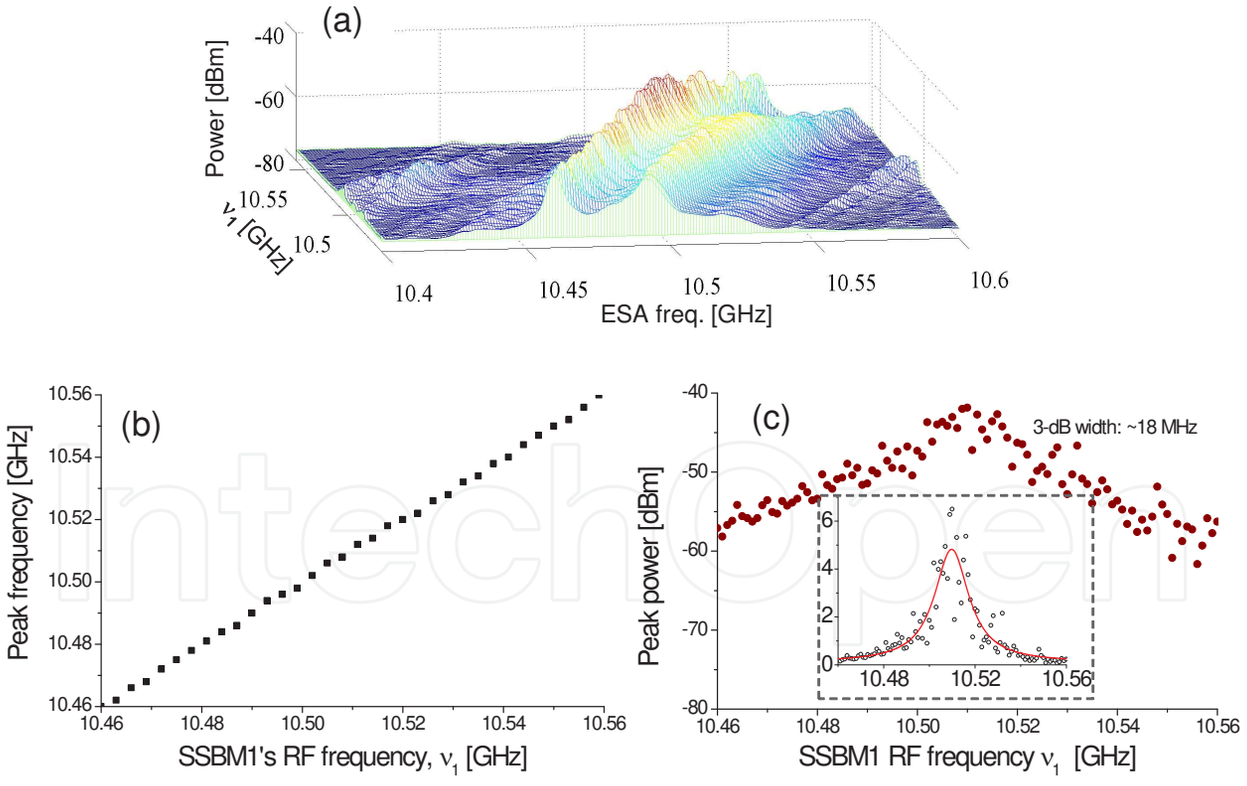

Figure 15. Characterization of the BDG reflection based on heterodyne detection. (a) 3D plot of electronic spectra of heterodyne detection when the pump-probe frequency offset (f_1-f_1') is scanned. Dependence of peak frequency (b) and power (c) of each spectrum on f_1-f_1'. The dashed inset denotes Lorentz fitting (solid curve) to the linear vertical scaled symbols in (c). (After Ref. [96]; © 2013 JJAP.)

pump-probe-based SBS process is well known to be changed when f_1-f_1' is swept [12], which is herein reflected by the measured power dependence [see Fig. 15(c)] since the diffraction/reflection wave sees the same change of the induced Brillouin gain. As shown in the inset of Fig. 15(c), Lorentz fitting provides the central frequency of ~10.510 GHz (just equal to the BFS), and Brillouin intrinsic linewidth of ~18 MHz. All experimental observation matches well the theoretical analysis of the BDG [97].

5.2. Complete discrimination of strain and temperature

As mentioned in **Section 5.1**, the BDG in a PMF can be generated by two coherent pump and probe waves in one principal polarization while readout by another wave deviated in frequency and separated spatially in the other principal polarization. This feature enables the BDG in a PMF working as a dynamic reflector for any optical wavelength of the readout wave by simply tuning the wavelengths of the pump and probe waves. The location of the BDG generation can be also dynamically assigned by changing the fiber's longitudinal structure [98] or programing the interaction position of the pump and probe waves [90, 99-103]. Up to date, the BDG in a PMF has been used for many applications in microwave photonics, all-optical signal processing, and Brillouin-based distributed sensors. For example, the BDG programmed in position or spectrum is very useful in microwave photonics of tunable optical delays [98, 104-106] or programmable microwave photonic filter [107]. Besides, it can also find significant applications in all-optical signal processing such as storing and compressing light [108], ultrawideband communications [109], and all-optical digital signal processing [110].

The first, but most successful, application of the BDG in a Panda-type PMF was demonstrated for complete discrimination of strain and temperature responses for Brillouin based distributed optical fiber sensing applications [89]. Figure 16 shows the basic experimental configuration of the high-precision BDG characterization, which can be used to precisely measure the birefringence of a PMF and to completely discriminate strain and temperature. The BDG generation is based on the pump-probe scheme, which is also the high-accuracy BGS characterization shown in Fig. 7(a). The BDG measurement is realized by the lock-in detection of the BDG reflection since the BDG is periodically chopped due to the chopping of the pump wave. The birefringence-determined frequency deviation defined in Eq. (40) is characterized within a standard error of Δf_{yx}=4 MHz, corresponding to a high-accuracy birefringence of ΔB=3 × 10^{-8}.

The principle of the complete discrimination is based on the dependence of the BFS on strain and temperature as introduced in Eq. (29) and the orthogonal dependence of the birefringence (B) or its determined frequency deviation on strain and temperature. This is because the residual tensile stress (σ_{xy}) determining the Panda-type PMF's birefringence scales with the ambient temperature (T_i):

$$B \propto \sigma_{xy} = k \cdot (\alpha_3 - \alpha_2) \cdot (T_{fic} - T_i), \tag{44}$$

where T_{fic} denotes the fictive temperature (e.g., 850 °C) of silica glass, α_3 (α_2) the thermal coefficient of B_2O_3-doped-silica stress-applying parts (pure-silica cladding), and k a constant

determined by the geometrical location of stress-applying parts in the fiber [111]. When temperature increases ($\Delta T=T_i$-25 > 0), the residual stress is released and thus the birefringence decreases as

$$\Delta B^T = -B_0 \cdot \frac{\Delta T}{T_{fic} - 25}, \tag{45}$$

where B_0 is the intrinsic birefringence at room temperature (T_i=25 °C).

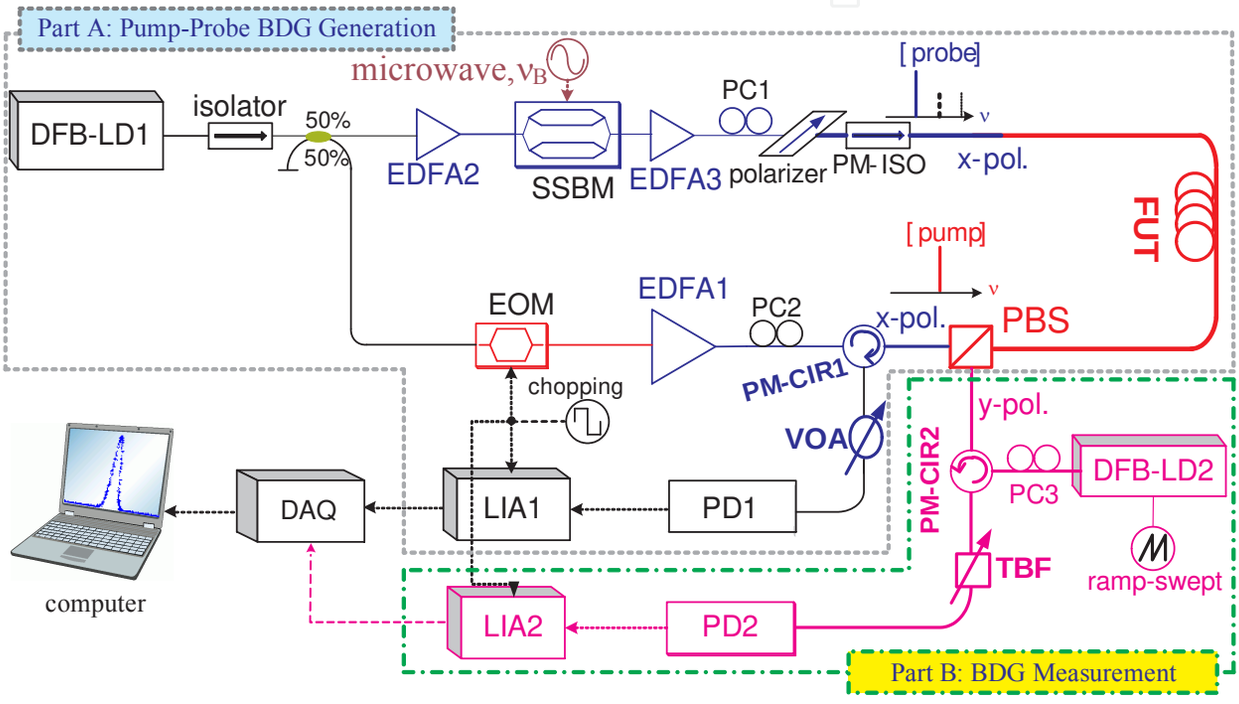

Figure 16. Configuration of the BDG characterization and strain-temperature discrimination. Part A, Pump-probe scheme to measure the BFS along *x*-axis and generate the BDG. Part B, Detection of the BDG diffraction spectrum to *y*-polarized readout wave. (After Ref. [89]; © 2009 OSA.)

In contrast, when an axial strain $\Delta\varepsilon$ is applied upon the fiber, additional stress is generated because the stress-applying parts and the cladding contract in the lateral direction differently due to their different Poisson's ratios ($\gamma_3>\gamma_2$) [111], the birefringence is enlarged with applied strain as

$$\Delta B^{\varepsilon} = +B_0 \cdot \frac{(\gamma_3 - \gamma_2)}{(\alpha_3 - \alpha_2)(T_{fic} - 25)} \cdot \Delta\varepsilon. \tag{46}$$

Consequently, the birefringence-determined frequency deviation (Δf) varies linearly with respect to temperature increase and to applied strain. Suppose that $C_f\varepsilon$ and C_f^T are the strain

http://dx.doi.org/10.5772/59145

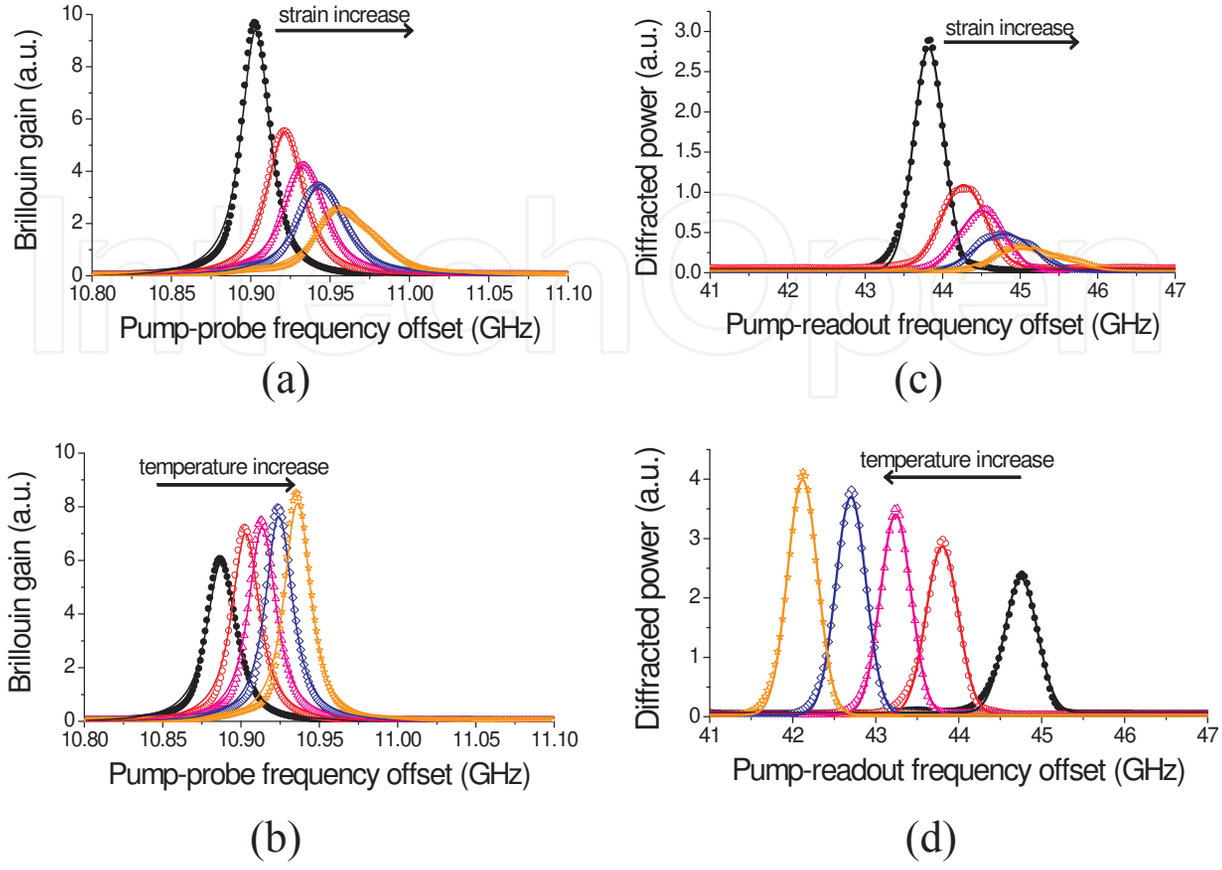

Figure 17. BGS (a, b) and BDG reflection (c, d) measured at various strain (a, c) and temperature (b, d). (After Ref. [89]; © 2009 OSA.)

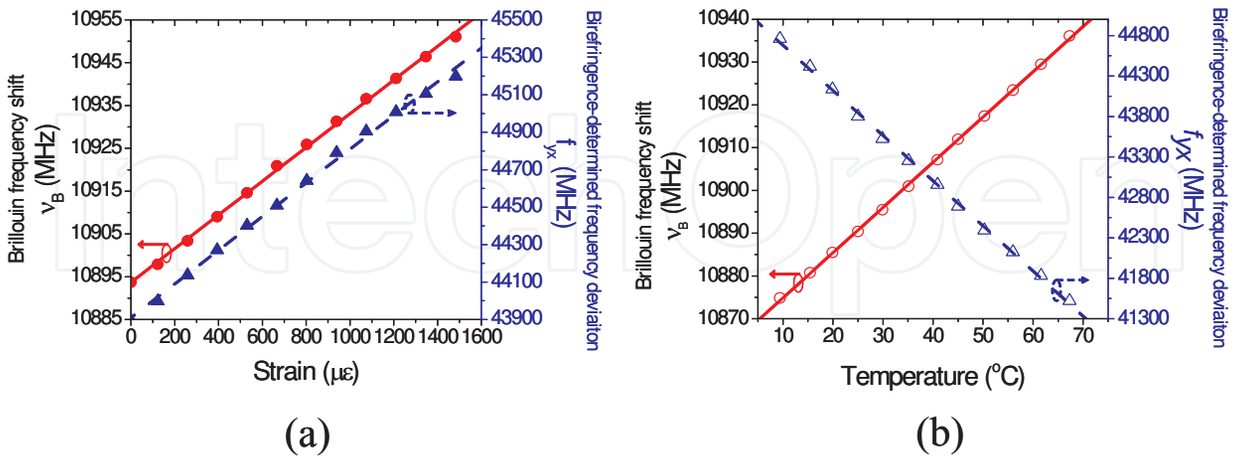

Figure 18. Brillouin frequency shift and birefringence-determined frequency deviation measured as functions of strain (a) and temperature (b). (After Ref. [89]; © 2009 OSA.)

coefficient and the temperature coefficient of the birefringence-determined frequency deviation, which can be deduced from Eqs. (40), (44), (45) and (46) as follows:

$$\begin{aligned} C_f^{\varepsilon} &= +\Delta f_0 \cdot \frac{(\gamma_3 - \gamma_2)}{(\alpha_3 - \alpha_2)(T_{fic} - 25)} \\ C_f^{T} &= -\Delta f_0 \cdot \frac{1}{(T_{fic} - 25)}, \end{aligned} \tag{47}$$

where Δf_0 is the frequency deviation at 25°C and in loose condition.

By jointly considering the BFS (ν_B) and the frequency deviation (Δf), one can deduce the strain ($\Delta\varepsilon$) and temperature (ΔT) referred to Eq. (37):

$$\begin{pmatrix} \Delta\varepsilon \\ \Delta T \end{pmatrix} = \frac{1}{C_\nu^{\varepsilon} \cdot C_f^{T} - C_\nu^{T} \cdot C_f^{\varepsilon}} \begin{pmatrix} C_f^{T} & -C_\nu^{T} \\ -C_f^{\varepsilon} & C_\nu^{\varepsilon} \end{pmatrix} \begin{pmatrix} \nu_B - \nu_{B0} \\ \Delta f - \Delta f_0 \end{pmatrix}, \tag{48}$$

where Δf_0 and ν_{B0} are the frequency deviation and the BFS at room temperature and in loose state.

In physics, the two phenomena/quantities, i.e. the ν_B and Δf of the fiber, are inherently independent. In mathematics, C_f^T has a sign opposite to those of other three coefficients, so that the denominator ($C\nu\varepsilon\ C_f^T$-$C\nu^T\ C_f\varepsilon$) of Eq. (48) has a significant value. The experimental results are depicted in Fig. 17 and Fig. 18, which give the two groups of coefficients ($C\nu\varepsilon$=+0.03938 MHz/$\mu\varepsilon$ and $C\nu^T$=+1.0580 MHz/°C; and $C_f\varepsilon$=+0.8995 MHz/$\mu\varepsilon$ and C_f^T=-55.8134 MHz/ °C). Putting above strain/temperature coefficients into Eq. (48), and taking the standard errors of the measurement system ($\Delta\nu_B$=0.1 MHz and Δf_{yx}=4 MHz, respectively) into account, the accuracy of the discrimination is given as high as $\Delta\varepsilon$=± 3.1 $\mu\varepsilon$ and ΔT=± 0.078 °C. Therefore, a complete discrimination of strain and temperature based on simultaneous measurement of the two quantities is ensured.

For distributed discrimination of strain and temperature, the localized BDG generation and readout in the PMF should be firstly proved to be effective. A correlation-based continuous-wave technique based on the BOCDA system [99] is used for random access and a pulse-based time-domain technique based on the BOTDA system [100] is employed for continuous access. It was found that the generation and readout waves based on the BOCDA system should be synchronously frequency-modulated because of the dispersion properties of all four waves (see Fig. 19) [112], including pump and probe waves, readout wave and acoustic wave (BDG as well).

The preliminary success of distributed discrimination of strain and temperature was realized by use of several lasers based on the BOCDA system [113] or the BOTDA system [114]. In [113], all pump, probe, and readout waves are synchronously modulated in frequency by sinusoidal functions to the two laser diodes. The measurement range of the distributed BGS and BDG is

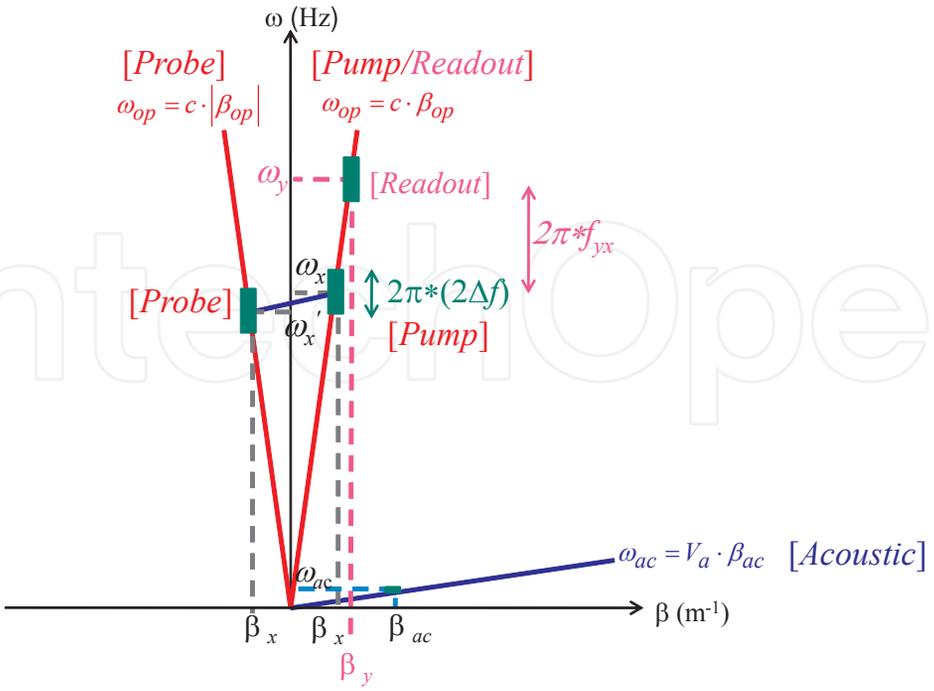

Figure 19. Dispersion properties of all optical (pump, probe and readout) and acoustic wave (Brillouin dynamic grating). (After Ref. [112]; © 2011 OSA.)

commonly given by the neighboring correlation peaks of the BOCDA system as defined in Eq. (35). Although the spatial resolution of the BGS measurement is still given by Eq. (34), that of the BDG reflection was thought to be determined by the BDG bandwidth (Δf_{yx}) as follows:

$$\Delta Z_{BDG} = \frac{c}{2nf_m} \cdot \frac{\Delta f_{yx}}{\pi \Delta f}. \tag{49}$$

The feasibility of distributed discrimination of strain and temperature was experimentally demonstrated with 10-cm spatial resolution. The f_m=12.429 MHz determines the nominal measurement range as d_m=8.35 m according to Eq. (35). For local BGS and BDG measurement, the Δf_B=1.5 GHz and Δf_D=10 GHz correspond to a nominal spatial resolution Δz_B=5 cm and Δz_D=8 cm [see Eq. (34) and Eq. (49)], respectively. As shown in Fig. 20(a), a ~8-m PMF sample is prepared, which consists of nine (A-I) cascaded fiber portions of 10-16 cm in length. The A, C, G and I portions were loosely laid at 25.1 °C for reference, while the B, D, F, and H portions were loosely inserted into a temperature-controlled water bath with 0.1-°C accuracy. The E portion was also inserted into the water bath and glued to a set of translation stages to load strain. The measured distribution of the changes of Δv_B and Δf_{yx} are summarized in Figs. 20(b) and 20(c), respectively. Referred to the characterized coefficients in Fig. 18 and the cross-sensitivity matrix in Eq. (48), the deducted distribution of temperature and strain along the fiber is depicted in Figs. 20(d) and 20(e), which clearly shows the feasibility of distributed discrimination of strain and temperature. In [114], all pump, probe, and readout waves are

pulsed in time domain; in turn, the BDG generation and readout as well as the BGS and BDG reflection are continuously localized by control of their relative delay towards the FUT and thus the local ν_B and Δf are detected for distributed discrimination of the strain and temperature responses.

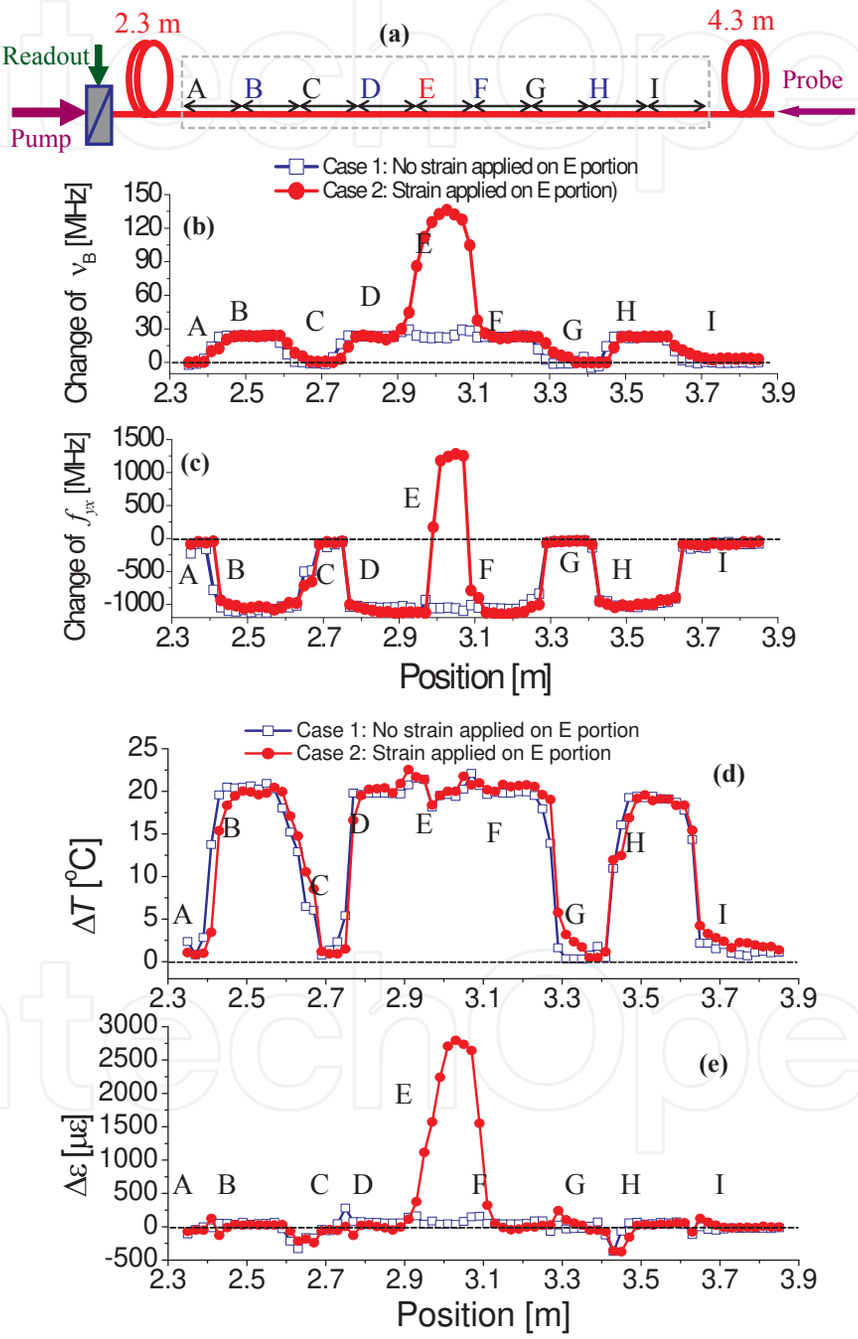

Figure 20. Preliminary experiment of distributed discrimination of strain and temperature based on two lasers modulated in frequency. (a) FUT configuration. Measured distribution of Brillouin frequency shift (b) and the birefringence-determined frequency deviation (c). Deduced distribution of temperature (d) and strain (e). (After Ref. [113]; © 2010 IEEE.)

http://dx.doi.org/10.5772/59145

One-laser-based Brillouin correlation-domain distributed discrimination system [112] by use of the sideband-generation technique was recently demonstrated to overcome the frequency fluctuation among the free-running lasers for pump, probe, and readout waves, and thus improve the accuracy of distributed discrimination of strain and temperature. Figure 21 represents the experimental setup. A 40-GHz intensity modulator (IM2) laid after the laser diode is driven by a radio frequency synthesizer (RF2 at ν_{RF2}) with a proper dc bias so as to generate double sidebands with suppressed carrier (DSB-SC). The optical filtering (FBG and tunable band-pass filter) is used to separate the two sidebands for the BDG generation and readout. By control of the RF1 (similar to Fig. 16), the BFS can be precisely measured and then fixed; by tuning of the RF2, the BDG reflection can be also precisely characterized; by simply change of the modulation frequency of the one laser diode, the location of the BGS and BDG can be swept for distributed measurement.

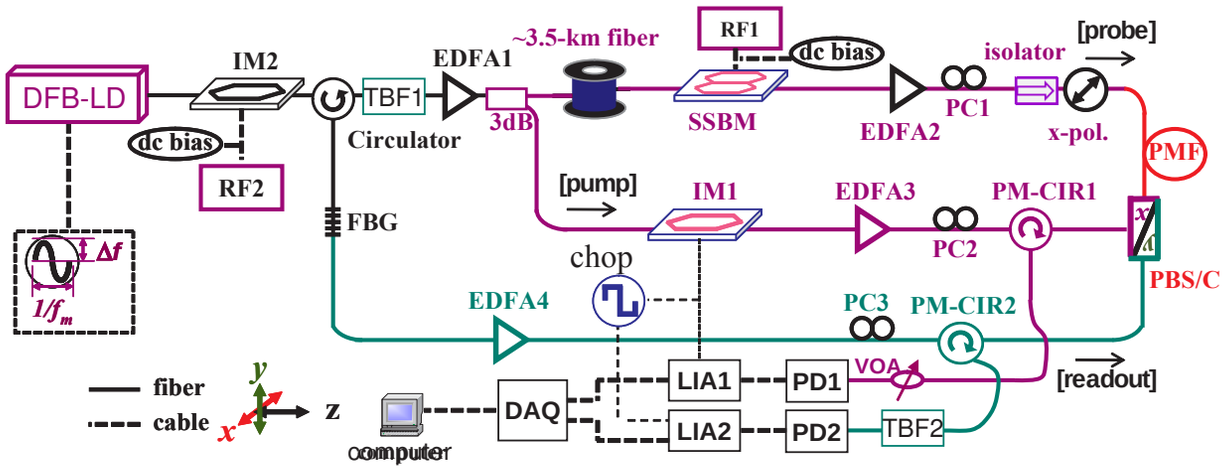

Figure 21. Experimental setup of the one-laser-based Brillouin correlation-domain distributed discrimination system. (After Ref. [112]; © 2011 OSA.)

Figure 22 shows the higher stability and accuracy (several MHz) of the one-laser scheme when compared to the two-laser scheme (several hundreds of MHz) both under no averaging process. Note that the one-laser scheme can also provide higher speed in the measurement of BGS and BDG and simpler measurement without sophisticated synchronization. Its distributed discrimination of strain and temperature was confirmed with the spatial resolution of ~10 cm and measurement range of ~5 m, which is depicted in Fig. 23 when the fiber was heated from 25 °C to 30 °C or/and the strain (ε=2000 $\mu\varepsilon$) was applied both at the location of 3.1 m. The measured results match well with the setting situation.

In order to overcome the tradeoff between the spatial resolution and measurement range always existing in the BOCDA system, a temporal gating [115] or a dual frequency modulation scheme [116] with a simple modification in Fig. 21 was used to elongate the measurement range of distributed discrimination of strain and temperature. For temporal gating scheme, the pulse modulation of RF2 makes the frequency-modulated pump, probe and readout waves optically pulsed in time and only one of the multiple correlation peaks are effectively generated in the

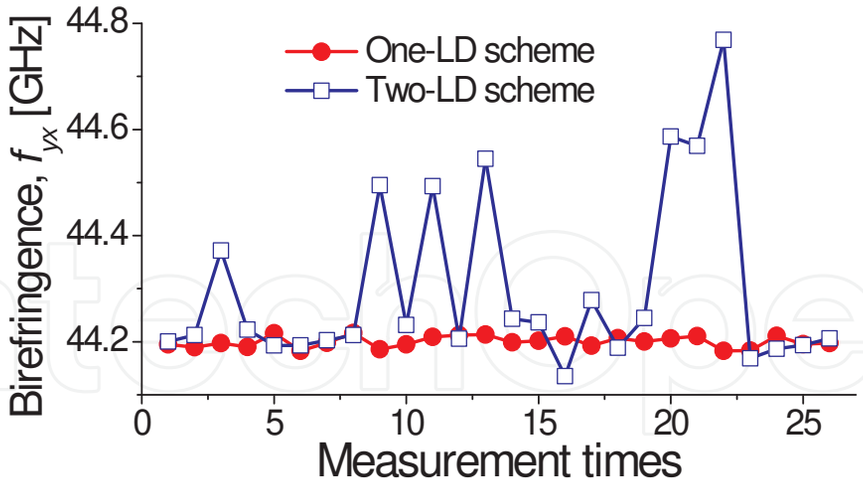

Figure 22. Comparison of the stability and accuracy of one-laser (solid dots) and two-laser (dashed squares) schemes of the BDG reflection. (After Ref. [112]; © 2011 OSA.)

FUT. For dual frequency modulation scheme, two sinusoidal functions are combined together to simultaneously modulate the optical frequencies of the pump, probe and readout waves. The greater modulation frequency ensures the higher spatial resolution while the lower modulation frequency realizes the longer measurement range. A 20 times [115] or 7 times [116] enlargement of the ratio between the measurement range and the spatial resolution was successfully demonstrated. It is expectable to achieve Brillouin optical correlation-domain distributed discrimination of strain and temperature having both a higher spatial resolution (better than 10 cm) and a longer measurement range (better than 1,000 m) by combining the dual frequency modulation scheme with the temporal gating scheme, which is now under study. Most recently, an apodization method under the assistance of intensity modulation was proposed to suppress the sidelobe of SOCF and enhance the spatial resolution of the strain-temperature discrimination by 4.5 times [117].

5.3. System improvement of sensing techniques

Many works have been involved in improving the system performance of BOTDA/BOTDR and BOCDA/BOCDR in terms of spatial resolution, measurement range, sensing speed and accuracy. In 1995, Bao *et al.* developed a Brillouin-loss-based BOTDA [118] by reversing the functions of the pulse laser and CW light. In other words, a strong CW light acts as a Brillouin pump wave and a pulse light with a scanned down-shifted frequency from that of the CW light works as a probe wave [119]. After monitoring the optical loss profile of the pump wave due to Brillouin interaction between the two light waves as a function of time or position along the fiber, a numerical signal processing of the poor SNR was used to achieve ~25 cm spatial resolution with a strain resolution of ~40 $\mu\varepsilon$ [120]. A pulse-pre-pump BOTDA (called PPP-BOTDA) was proposed to realize cm-order spatial resolution by using a wide pulse (larger than 10 ns) followed by a narrow pulse (smaller than 1 ns) [121], which is in principle similar to the BOTDA with a pulse generated by a finite extinction ratio [122]. A dark-pulse-based BOTDA was later presented to hopefully obtain 2-cm spatial resolution [123, 124], which

http://dx.doi.org/10.5772/59145

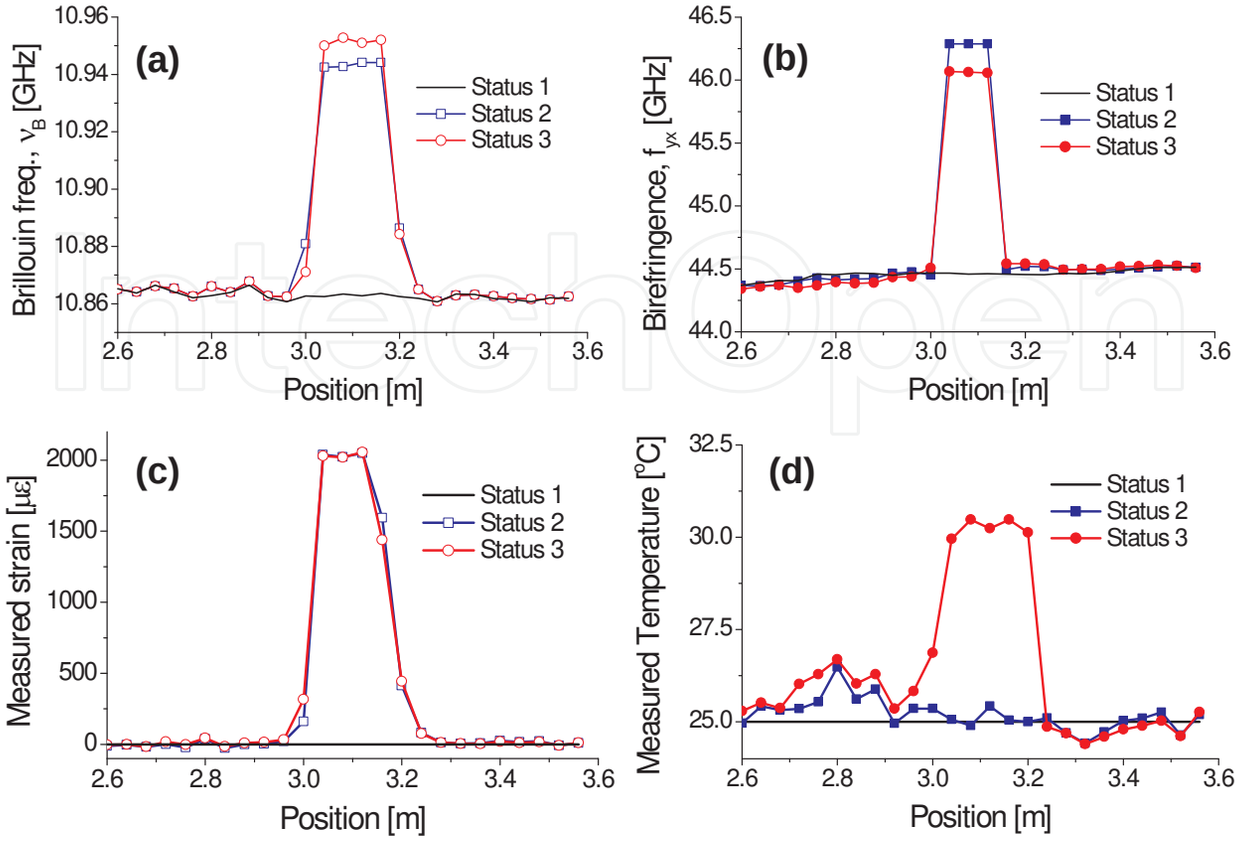

Figure 23. Experimental results of high-accuracy distributed discrimination of strain and temperature based on one-laser scheme. Distribution of Brillouin frequency shift (a), the birefringence-determined frequency deviation (b), strain (c), and temperature (d). (After Ref. [112]; © 2011 OSA.)

suffers a neglectful influence of the acoustic lifetime (~10 ns) but an experimental difficulty of high-qualify dark pulse and a scarified measurement range due to the pump depletion of the dc base. A new scheme by combination of the PPP-BOTDA and dark-pulse-based BOTDA [125] was demonstrated to achieve higher spatial resolution as well as better frequency resolution. Taking the similar principle of the PPP-BOTDA technique, a BDG-based BOTDA was proposed to obtain cm-order or sub-cm-order spatial resolution [126-128]. The only difference lies on the fact that the Brillouin interaction in the BDG-based BOTDA is generated by a long pulse along one principal polarization state (the BDG generation process) and detected by a short pulse along the orthogonal polarization state (the BDG readout process). Another type of the modified BOTDA with higher spatial resolution of less than 1 meter is based on a group of pulses, called differential pulse-width pair BOTDA (DPP-BOTDA) [129-132] or Brillouin echo BOTDA [133, 134]. In DPP-BOTDA, a pair of pulses with a small difference of the pulse widths are successively launched into the FUT; the Brillouin interaction is recorded for twice and a subtraction is performed to achieve the sensing trace with the high spatial resolution determined by the small pulse-width difference. The spatial resolution of BOTDR has been also more or less improved by an experimental optimization or signal processing process [135-137].

Although BOTDA and BOTDR are excellent for long sensing range (such as kilometers or tens of km), they still suffer the physical limitation of maximum range due to the nature of fiber loss and/or the Brillouin depletion effect. There are two typical methods, i.e. Raman-assisted BOTDR[138-140] or Raman-assisted BOTDA[141-145] and coded BOTDR[146] or coded BOTDA[147-151], to improve the poor SNR and achieve a very long sensing range. The best performance of the sensing range (longer than 120 km) [152, 153] with an acceptable spatial resolution (1 m or 2 m) has been renovated by combination of Raman assistance and coding although the system becomes extremely complicated. Most recently, specially-designed EDFA repeaters were used to extend the sensing measurements of BOTDA to more than 300 km [154]. Some efforts were also made to study the influence of Brillouin depletion on the maximum range of BOTDA [41] and to avoid it to some extent by use of Stokes together with anti-Stokes wave as Brillouin probe [155, 156].

BOCDA and BOCDR systems have natural advantages of high spatial resolution without any dependence on the acoustic lifetime and random programmable accessibility of the sensing location. Except for the great innovation of Brillouin optical correlation-domain distributed discrimination of strain and temperature introduced in **Section 5.2**, advances in BOCDA and BOCDR systems have also boosted in the past decade. The polarization disturbance along the FUT has been effectively solved by use of the polarization diversity scheme to the BOCDA system [157]. A complicated double-lock-in detection was proposed to improve the SNR of the BOCDA system [69, 158] although a modified lock-in detection based on variable chopping frequency [159] or a simplified but equivalent BOCDA system based on combination of Brillouin gain and loss [34] was later proposed. The existence of a big noise floor originated from the uncorrelated locations strongly limits the maximum strain or temperature change to be detected, which has been eliminated by use of intensity modulation for SOCF apodization [160, 161] or differential measurement scheme based on external phase modulation [162]. The measurement range of BOCDA [116, 163, 164] or BOCDR [165, 166] was extended by use of temporal gating or double frequency modulation scheme, respectively. Besides, combination of time-domain and correlation domain techniques [167, 168] has been proposed to enlarge the measurement range of the BOCDA [169] based on external phase modulation. The distributed sensing speed with cm-order spatial resolution [170-172] has been substantially increased to several Hertz along the entire FUT by optimizing the position sweeping and the BGS mapping although the local sensing speed of the BOCDA [173-175] or BOCDR [176] was well-known to be high at the random-accessed sensing location.

6. Conclusions

We have presented an essential overview of Brillouin scattering in optical fibers and Brillouin based distributed optical fiber sensors. Started from the basic principle of Brillouin scattering in optical fibers, the basic mechanism of Brillouin based distributed optical fiber sensors (linear dependence of Brillouin frequency shift on strain and temperature) and the two different groups of Brillouin based distributed optical fiber sensors (time domain: BOTDA/BOTDR; correlation domain: BOCDA/BOCDR) were described in detail. The difficulties and challenges

of how to simultaneously sense strain and temperature were demonstrated and the physical limitation of the sensing abilities (spatial resolution, measurement range, accuracy etc.) were introduced, respectively. Finally, we summarized recent advances of this field towards the solutions to those difficulties and challenges.

It is valuable to address that Brillouin based distributed optical fiber sensors are nowadays in a high technical level, which have been attracting industrial companies to commercialize for structural health monitoring in civil structures, aerospace, energy (gas, oil) pipeline, and engineers (power supply).

Acknowledgements

This work was partially supported by National Natural Science Foundation of China (Grant Nos. 61007052 and 61127016), Shanghai Pujiang Program (Grant No. 12PJ1405600), and by the State Key Lab Project of Shanghai Jiao Tong University under Grant GKZD030033. Professor Kazuo Hotate at the University of Tokyo and Professor Zuyuan He at Shanghai Jiao Tong University are gratefully acknowledged for their contributions in many relevant works presented in this chapter.

Author details

Weiwen Zou*, Xin Long and Jianping Chen

*Address all correspondence to: wzou@sjtu.edu.cn

State Key Laboratory of Advanced Optical Communication Systems and Networks, Department of Electronic Engineering, Shanghai Jiao Tong University, Shanghai, China

References

[1] G. P. Agrawal, *Nonlinear Fiber Optics,* 5th ed. (Academic Press, 2012).

[2] E. Ippen and R. Stolen, "Stimulated Brillouin scattering in optical fibers," Appl. Phys. Lett. 21, 539-541 (1972).

[3] R. Shelby, M. Levenson, and P. Bayer, "Resolved forward Brillouin scattering in optical fibers," Phys. Rev. Lett. 54, 939-942 (1985).

[4] Y. Mizuno and K. Nakamura, "Brillouin Scattering in Polymer Optical Fibers: Fundamental Properties and Potential Use in Sensors," Polymers 3, 886-898 (2011).

[5] A. L. Gaeta and R. W. Boyd, "Stochastic dynamics of stimulated Brillouin scattering in an optical fiber," Phys. Rev. A 44, 3205-3209 (1991).

[6] R. B. Jenkins, R. M. Sova, and R. I. Joseph, "Steady-state noise analysis of spontaneous and stimulated Brillouin scattering in optical fibers," J. Lightwave Technol. 25, 763-770 (2007).

[7] A. S. Pine, "Brillouin Scattering Study of Acoustic Attenuation in Fused Quartz," Physical Review 185, 1187-1193 (1969).

[8] W. Zou, Z. He, and K. Hotate, "Two-dimensional finite-element modal analysis of Brillouin gain spectra in optical fibers," Photonics Technology Letters, IEEE 18, 2487-2489 (2006).

[9] A. Kobyakov, M. Sauer, and D. Chowdhury, "Stimulated Brillouin scattering in optical fibers," Advances in optics and photonics 2, 1-59 (2010).

[10] A. Kobyakov, S. Kumar, D. Q. Chowdhury, A. B. Ruffin, M. Sauer, S. R. Bickham, and R. Mishra, "Design concept for optical fibers with enhanced SBS threshold," Opt. Express 13, 5338-5346 (2005).

[11] Y. Koyamada, S. Sato, S. Nakamura, H. Sotobayashi, and W. Chujo, "Simulating and designing brillouin gain spectrum in single-mode fibers," J. Lightwave Technol. 22, 631-639 (2004).

[12] W. Zou, Z. He, A. D. Yablon, and K. Hotate, "Dependence of Brillouin frequency shift in optical fibers on draw-induced residual elastic and inelastic strains," Photonics Technology Letters, IEEE 19, 1389-1391 (2007).

[13] W. Zou, Z. Y. He, and K. Hotate, "Acoustic modal analysis and control in w-shaped triple-layer optical fibers with highly-germanium-doped core and F-doped inner cladding," Opt. Express 16, 10006-10017 (2008).

[14] L. Tartara, C. Codemard, J.-N. Maran, R. Cherif, and M. Zghal, "Full modal analysis of the Brillouin gain spectrum of an optical fiber," Opt. Commun. 282, 2431-2436 (2009).

[15] B. Ward and J. Spring, "Finite element analysis of Brillouin gain in SBS-suppressing optical fibers with non-uniform acoustic velocity profiles," Opt. Express 17, 15685-15699 (2009).

[16] Y. S. Mamdem, X. Phéron, F. Taillade, Y. Jaoüen, R. Gabet, V. Lanticq, G. Moreau, A. Boukenter, Y. Ouerdane, and S. Lesoille, "Two-dimensional FEM analysis of Brillouin Gain Spectra in acoustic guiding and antiguiding single mode optical fibers," in *COMSOL Conference*, 2010),

[17] S. Dasgupta, F. Poletti, S. Liu, P. Petropoulos, D. J. Richardson, L. Gruner-Nielsen, and S. Herstrøm, "Modeling Brillouin Gain Spectrum of solid and microstructured

optical fibers using a finite element method," Lightwave Technology, Journal of 29, 22-30 (2011).

[18] X. Qian, B. Han, and Q. Wang, "Numerical Research on Gain Spectrum of Stimulated Brillouin Scattering in Photonics Crystal Fiber," Instrumentation Science & Technology 41, 175-186 (2013).

[19] L. Dong, "Formulation of a complex mode solver for arbitrary circular acoustic waveguides," J. Lightwave Technol. 28, 3162-3175 (2010).

[20] P. D. Dragic and B. G. Ward, "Accurate modeling of the intrinsic Brillouin linewidth via finite-element analysis," Photonics Technology Letters, IEEE 22, 1698-1700 (2010).

[21] C. G. Carlson, R. B. Ross, J. M. Schafer, J. B. Spring, and B. G. Ward, "Full vectorial analysis of Brillouin gain in random acoustically microstructured photonic crystal fibers," Phys. Rev. B 83, 235110 (2011).

[22] Y. Okawachi, M. S. Bigelow, J. E. Sharping, Z. M. Zhu, A. Schweinsberg, D. J. Gauthier, R. W. Boyd, and A. L. Gaeta, "Tunable all-optical delays via Brillouin slow light in an optical fiber," Phys. Rev. Lett. 94(2005).

[23] K. Y. Song, M. G. Herraez, and L. Thevenaz, "Observation of pulse delaying and advancement in optical fibers using stimulated Brillouin scattering," Opt. Express 13, 82-88 (2005).

[24] N. Shibata, K. Okamoto, and Y. Azuma, "Longitudinal acoustic modes and Brillouin-gain spectra for GeO< sub> 2</sub>-doped-core single-mode fibers," JOSA B 6, 1167-1174 (1989).

[25] M. Nikles, L. Thevenaz, and P. A. Robert, "Brillouin gain spectrum characterization in single-mode optical fibers," Lightwave Technology, Journal of 15, 1842-1851 (1997).

[26] A. Yeniay, J.-M. Delavaux, and J. Toulouse, "Spontaneous and Stimulated Brillouin Scattering Gain Spectra in Optical Fibers," J. Lightwave Technol. 20, 1425 (2002).

[27] W. Zou, Z. He, and K. Hotate, "Experimental study of Brillouin scattering in fluorine-doped single-mode optical fibers," Opt. Express 16, 18804-18812 (2008).

[28] R. G. Smith, "Optical Power Handling Capacity of Low Loss Optical Fibers as Determined by Stimulated Raman and Brillouin Scattering," Appl. Optics 11, 2489-2494 (1972).

[29] V. I. Kovalev and R. G. Harrison, "Threshold for stimulated Brillouin scattering in optical fiber," Opt. Express 15, 17625-17630 (2007).

[30] N. Rowell, P. Thomas, H. Van Driel, and G. Stegeman, "Brillouin spectrum of single-mode optical fibers," Appl. Phys. Lett. 34, 139-141 (1979).

[31] S. M. Maughan, H. H. Kee, and T. P. Newson, "Simultaneous distributed fibre temperature and strain sensor using microwave coherent detection of spontaneous Brillouin backscatter," Measurement Science and Technology 12, 834 (2001).

[32] Y. Koyamada, "Proposal and simulation of double-pulse brillouin optical time-domain analysis for measuring distributed strain and temperature with cm spatial resolution in km-long fiber," IEICE Trans. Commun. E90B, 1810-1815 (2007).

[33] X. Bao, D. J. Webb, and D. A. Jackson, "32-km distributed temperature sensor based on Brillouin loss in an optical fiber," Opt. Lett. 18, 1561-1563 (1993).

[34] W. Zou, C. J. Jin, and J. P. Chen, "Distributed Strain Sensing Based on Combination of Brillouin Gain and Loss Effects in Brillouin Optical Correlation Domain Analysis," Appl. Phys. Express 5(2012).

[35] K. Higuma, S. Oikawa, Y. Hashimoto, H. Nagata, and M. Izutsu, "X-cut lithium niobate optical single-sideband modulator," Electron. Lett. 37, 515-516 (2001).

[36] A. Loayssa, R. Hernández, D. Benito, and S. Galech, "Characterization of stimulated Brillouin scattering spectra by use of optical single-sideband modulation," Opt. Lett. 29, 638-640 (2004).

[37] W. Zou, Z. Y. He, M. Kishi, and K. Hotate, "Stimulated Brillouin scattering and its dependences on strain and temperature in a high-delta optical fiber with F-doped depressed inner cladding," Opt. Lett. 32, 600-602 (2007).

[38] V. I. Kovalev and R. G. Harrison, "Observation of inhomogeneous spectral broadening of stimulated Brillouin scattering in an optical fiber," Phys. Rev. Lett. 85, 1879 (2000).

[39] Y. Takushima and K. Kikuchi, "Spectral gain hole burning and modulation instability in a Brillouin fiber amplifier," Opt. Lett. 20, 34-36 (1995).

[40] L. Stépien, S. Randoux, and J. Zemmouri, "Origin of spectral hole burning in Brillouin fiber amplifiers and generators," Phys. Rev. A 65, 053812 (2002).

[41] L. Thévenaz, S. F. Mafang, and J. Lin, "Effect of pulse depletion in a Brillouin optical time-domain analysis system," Opt. Express 21, 14017-14035 (2013).

[42] X. Long, W. Zou, H. Li, and J. Chen, "Critical condition for spectrum distortion of pump–probe-based stimulated Brillouin scattering in an optical fiber," Appl. Phys. Express 7, 082501 (2014).

[43] T. Horiguchi and M. Tateda, "BOTDA-nondestructive measurement of single-mode optical fiber attenuation characteristics using Brillouin interaction: Theory," Lightwave Technology, Journal of 7, 1170-1176 (1989).

[44] T. Horiguchi, T. Kurashima, and M. Tateda, "Tensile strain dependence of Brillouin frequency shift in silica optical fibers," Photonics Technology Letters, IEEE 1, 107-108 (1989).

[45] T. Kurashima, T. Horiguchi, and M. Tateda, "Thermal effects of Brillouin gain spectra in single-mode fibers," Photonics Technology Letters, IEEE 2, 718-720 (1990).

[46] http://www.itu.int/rec/T-REC-G/en.

[47] C. K. Jen, C. Neron, A. Shang, K. Abe, L. Bonnell, and J. Kushibiki, "Acoustic characterization of silica glasses," Journal of the American Ceramic Society 76, 712-716 (1993).

[48] S. P. Timoshenko and J. Goodier, *Theory of elasticity* (2011).

[49] W. Zou, Z. He, and K. Hotate, "Investigation of Strain-and Temperature-Dependences of Brillouin Frequency Shifts in GeO< sub> 2</sub>-Doped Optical Fibers," J. Lightwave Technol. 26, 1854-1861 (2008).

[50] R. W. Tkach, A. R. Chraplyvy, and R. Derosier, "Spontaneous Brillouin scattering for single-mode optical-fibre characterisation," Electron. Lett. 22, 1011-1013 (1986).

[51] N. Shibata, R. G. Waarts, and R. P. Braun, "Brillouin-gain spectra for single-mode fibers having pure-silica, GeO 2-doped, and P 2O5-doped cores," Opt. Lett. 12, 269-271 (1987).

[52] T. Horiguchi, T. Kurashima, and M. Tateda, "A technique to measure distributed strain in optical fibers," Photonics Technology Letters, IEEE 2, 352-354 (1990).

[53] T. Kurashima, T. Horiguchi, H. Izumita, S.-i. Furukawa, and Y. Koyamada, "Brillouin optical-fiber time domain reflectometry," IEICE Trans. Commun. 76, 382-390 (1993).

[54] T. Horiguchi, T. Kurashima, and Y. Koyamada, "Measurement of temperature and strain distribution by Brillouin frequency shift in silica optical fibers," in *Fibers' 92*, (International Society for Optics and Photonics, 1993), 2-13.

[55] M. Niklès, L. Thévenaz, and P. A. Robert, "Simple distributed fiber sensor based on Brillouin gain spectrum analysis," Opt. Lett. 21, 758-760 (1996).

[56] K. Shimizu, T. Horiguchi, Y. Koyamada, and T. Kurashima, "Coherent self-heterodyne Brillouin OTDR for measurement of Brillouin frequency shift distribution in optical fibers," Lightwave Technology, Journal of 12, 730-736 (1994).

[57] D. Garcus, T. Gogolla, K. Krebber, and F. Schliep, "Brillouin optical-fiber frequency-domain analysis for distributed temperature and strain measurements," Lightwave Technology, Journal of 15, 654-662 (1997).

[58] D. Garus, K. Krebber, F. Schliep, and T. Gogolla, "Distributed sensing technique based on Brillouin optical-fiber frequency-domain analysis," Opt. Lett. 21, 1402-1404 (1996).

[59] K. Hotate and T. Hasegawa, "Measurement of Brillouin Gain Spectrum Distribution along an Optical Fiber Using a Correlation-Based Technique--Proposal, Experiment and Simulation," IEICE Trans. Electron. 83, 405-412 (2000).

[60] K. Hotate and M. Tanaka, "Distributed fiber Brillouin strain sensing with 1-cm spatial resolution by correlation-based continuous-wave technique," Photonics Technology Letters, IEEE 14, 179-181 (2002).

[61] Y. Mizuno, W. Zou, Z. He, and K. Hotate, "Proposal of Brillouin optical correlation-domain reflectometry (BOCDR)," Opt. Express 16, 12148-12153 (2008).

[62] K.-Y. Song and K. Hotate, "Brillouin optical correlation domain analysis in linear configuration," Photonics Technology Letters, IEEE 20, 2150-2152 (2008).

[63] W. Zou, Z. He, and K. Hotate, "Single-End-Access Correlation-Domain Distributed Fiber-Optic Sensor Based on Stimulated Brillouin Scattering," J. Lightwave Technol. 28, 2736-2742 (2010).

[64] Y. Mizuno, W. W. Zou, Z. Y. He, and K. Hotate, "Operation of Brillouin Optical Correlation-Domain Reflectometry: Theoretical Analysis and Experimental Validation," J. Lightwave Technol. 28, 3300-3306 (2010).

[65] K. Hotate and O. Kamatani, "Optical coherence domain reflectometry by synthesis of coherence function," Lightwave Technology, Journal of 11, 1701-1710 (1993).

[66] K. Hotate and T. Okugawa, "Optical information processing by synthesis of the coherence function," Lightwave Technology, Journal of 12, 1247-1255 (1994).

[67] R. Lang and K. Kobayashi, "External optical feedback effects on semiconductor injection laser properties," Quantum Electronics, IEEE Journal of 16, 347-355 (1980).

[68] Y. Mizuno, Z. He, and K. Hotate, "One-end-access high-speed distributed strain measurement with 13-mm spatial resolution based on Brillouin optical correlation-domain reflectometry," Photonics Technology Letters, IEEE 21, 474-476 (2009).

[69] K. Y. Song, Z. Y. He, and K. Hotate, "Distributed strain measurement with millimeter-order spatial resolution based on Brillouin optical correlation domain analysis," Opt. Lett. 31, 2526-2528 (2006).

[70] K. Hotate and S. S. Ong, "Distributed dynamic strain measurement using a correlation-based Brillouin sensing system," Photonics Technology Letters, IEEE 15, 272-274 (2003).

[71] K.-Y. Song and K. Hotate, "Distributed fiber strain sensor with 1 kHz sampling rate based on Brillouin optical correlation domain analysis," in *Optics East 2007*, (International Society for Optics and Photonics, 2007), 67700J-67700J-67708.

[72] M. Alahbabi, Y. Cho, and T. Newson, "Simultaneous temperature and strain measurement with combined spontaneous Raman and Brillouin scattering," Opt. Lett. 30, 1276-1278 (2005).

[73] G. Bolognini, M. A. Soto, and F. Di Pasquale, "Simultaneous distributed strain and temperature sensing based on combined Raman–Brillouin scattering using Fabry–Perot lasers," Measurement Science and Technology 21, 094025 (2010).

[74] M. Taki, A. Signorini, C. Oton, T. Nannipieri, and F. Di Pasquale, "Hybrid Raman/ Brillouin-optical-time-domain-analysis-distributed optical fiber sensors based on cyclic pulse coding," Opt. Lett. 38, 4162-4165 (2013).

[75] D.-P. Zhou, W. Li, L. Chen, and X. Bao, "Distributed Temperature and Strain Discrimination with Stimulated Brillouin Scattering and Rayleigh Backscatter in an Optical Fiber," Sensors 13, 1836-1845 (2013).

[76] C. Lee, P. Chiang, and S. Chi, "Utilization of a dispersion-shifted fiber for simultaneous measurement of distributed strain and temperature through Brillouin frequency shift," Photonics Technology Letters, IEEE 13, 1094-1096 (2001).

[77] L. F. Zou, X. Y. Bao, V. S. Afshar, and L. Chen, "Dependence of the Brillouin frequency shift on strain and temperature in a photonic crystal fiber," Opt. Lett. 29, 1485-1487 (2004).

[78] T. Parker, M. Farhadiroushan, V. Handerek, and A. Rogers, "Temperature and strain dependence of the power level and frequency of spontaneous Brillouin scattering in optical fibers," Opt. Lett. 22, 787-789 (1997).

[79] M. Alahbabi, Y. T. Cho, and T. P. Newson, "Comparison of the methods for discriminating temperature and strain in spontaneous Brillouin-based distributed sensors," Opt. Lett. 29, 26-28 (2004).

[80] M. Belal and T. P. Newson, "Experimental Examination of the Variation of the Spontaneous Brillouin Power and Frequency Coefficients Under the Combined Influence of Temperature and Strain," J. Lightwave Technol. 30, 1250-1255 (2012).

[81] X. Y. Bao, Q. R. Yu, and L. Chen, "Simultaneous strain and temperature measurements with polarization-maintaining fibers and their error analysis by use of a distributed Brillouin loss system," Opt. Lett. 29, 1342-1344 (2004).

[82] H. Naruse and M. Tateda, "Trade-off between the spatial and the frequency resolutions in measuring the power spectrum of the Brillouin backscattered light in an optical fiber," Appl. Optics 38, 6516-6521 (1999).

[83] S.-B. Cho, Y.-G. Kim, J.-S. Heo, and J.-J. Lee, "Pulse width dependence of Brillouin frequency in single mode optical fibers," Opt. Express 13, 9472-9479 (2005).

[84] M. A. Soto and L. Thévenaz, "Modeling and evaluating the performance of Brillouin distributed optical fiber sensors," Opt. Express 21, 31347-31366 (2013).

[85] A. Minassian, G. J. Crofts, and M. J. Damzen, "Spectral filtering of gain gratings and spectral evolution of holographic laser oscillators," Quantum Electronics, IEEE Journal of 36, 802-809 (2000).

[86] X. Fan, Z. He, Y. Mizuno, and K. Hotate, "Bandwidth-adjustable dynamic grating in erbium-doped fiber by synthesis of optical coherence function," Opt. Express 13, 5756-5761 (2005).

[87] R. Elsner, R. Ullmann, A. Heuer, R. Menzel, and M. Ostermeyer, "Two-dimensional modeling of transient gain gratings in saturable gain media," Opt. Express 20, 6887-6896 (2012).

[88] K.-Y. Song and K. Hotate, "All-optical dynamic grating generation based on Brillouin scattering in polarization maintaining fiber," in *19th International Conference on Optical Fibre Sensors*, (International Society for Optics and Photonics, 2008), 70043T-70043T-70044.

[89] W. Zou, Z. He, and K. Hotate, "Complete discrimination of strain and temperature using Brillouin frequency shift and birefringence in a polarization-maintaining fiber," Opt. Express 17, 1248-1255 (2009).

[90] Y. Dong, L. Chen, and X. Bao, "Truly distributed birefringence measurement of polarization-maintaining fibers based on transient Brillouin grating," Opt. Lett. 35, 193-195 (2010).

[91] S. Li, M.-J. Li, and R. S. Vodhanel, "All-optical Brillouin dynamic grating generation in few-mode optical fiber," Opt. Lett. 37, 4660-4662 (2012).

[92] K. Y. Song, "Operation of Brillouin dynamic grating in single-mode optical fibers," Opt. Lett. 36, 4686-4688 (2011).

[93] W. Zou and J. P. Chen, "All-optical generation of Brillouin dynamic grating based on multiple acoustic modes in a single-mode dispersion-shifted fiber," Opt. Express 21, 14771-14779 (2013).

[94] R. Pant, E. Li, C. G. Poulton, D.-Y. Choi, S. Madden, B. Luther-Davies, and B. J. Eggleton, "Observation of Brillouin dynamic grating in a photonic chip," Opt. Lett. 38, 305-307 (2013).

[95] K. O. Hill and G. Meltz, "Fiber Bragg grating technology fundamentals and overview," Lightwave Technology, Journal of 15, 1263-1276 (1997).

[96] W. Zou and J. Chen, "Spectral Analysis of Brillouin Dynamic Grating Based on Heterodyne Detection," Appl. Phys. Express 6, 122503 (2013).

[97] D. P. Zhou, L. Chen, and X. Y. Bao, "Polarization-decoupled four-wave mixing based on stimulated Brillouin scattering in a polarization-maintaining fiber," J. Opt. Soc. Am. B-Opt. Phys. 30, 821-828 (2013).

[98] K. Y. Song, K. Lee, and S. B. Lee, "Tunable optical delays based on Brillouin dynamic grating in optical fibers," Opt. Express 17, 10344-10349 (2009).

[99] W. Zou, Z. He, K.-Y. Song, and K. Hotate, "Correlation-based distributed measurement of a dynamic grating spectrum generated in stimulated Brillouin scattering in a polarization-maintaining optical fiber," Opt. Lett. 34, 1126-1128 (2009).

[100] K. Y. Song, W. Zou, Z. He, and K. Hotate, "Optical time-domain measurement of Brillouin dynamic grating spectrum in a polarization-maintaining fiber," Opt. Lett. 34, 1381-1383 (2009).

[101] Y. Antman, N. Primerov, J. Sancho, L. Thévenaz, and A. Zadok, "Localized and stationary dynamic gratings via stimulated Brillouin scattering with phase modulated pumps," Opt. Express20 (7), 7807-7821 (2012).

[102] M. Santagiustina and L. Ursini, "Dynamic Brillouin gratings permanently sustained by chaotic lasers," Opt. Lett. 37, 893-895 (2012).

[103] Y. Antman, L. Yaron, T. Langer, M. Tur, N. Levanon, and A. Zadok, "Experimental demonstration of localized Brillouin gratings with low off-peak reflectivity established by perfect Golomb codes," Opt. Lett. 38, 4701-4704 (2013).

[104] Y. Antman, N. Primerov, J. Sancho, L. Thevenaz, and A. Zadok, "Long variable delay and distributed sensing using stationary and localized Brillouin dynamic gratings," in *Optical Fiber Communication Conference*, (Optical Society of America, 2012),

[105] Y. Antman, N. Primerov, J. Sancho, L. Thévenaz, and A. Zadok, "Variable delay using stationary and localized Brillouin dynamic gratings," in *SPIE OPTO*, (International Society for Optics and Photonics, 2012), 82730C-82730C-82738.

[106] S. Chin and L. Thevenaz, "Tunable photonic delay lines in optical fibers," Laser Photon. Rev. 6, 724-738 (2012).

[107] J. Sancho, N. Primerov, S. Chin, Y. Antman, A. Zadok, S. Sales, and L. Thévenaz, "Tunable and reconfigurable multi-tap microwave photonic filter based on dynamic Brillouin gratings in fibers," Opt. Express20 (6), 6157-6162 (2012).

[108] H. G. Winful, "Chirped Brillouin dynamic gratings for storing and compressing light," Opt. Express 21, 10039-10047 (2013).

[109] L. Ursini and M. Santagiustina, "Applications of the Dynamic Brillouin Gratings to Ultrawideband Communications," IEEE Photonics Technol. Lett. 25, 1347-1349 (2013).

[110] M. Santagiustina, S. Chin, N. Primerov, L. Ursini, and L. Thévenaz, "All-optical signal processing using dynamic Brillouin gratings," Scientific reports 3(2013).

[111] K. Chiang, D. Wong, and P. Chu, "Strain-induced birefringence in a highly birefringent optical fibre," Electron. Lett. 26, 1344-1346 (1990).

[112] W. Zou, Z. He, and K. Hotate, "One-laser-based generation/detection of Brillouin dynamic grating and its application to distributed discrimination of strain and temperature," Opt. Express 19, 2363-2370 (2011).

[113] W. Zou, Z. He, and K. Hotate, "Demonstration of Brillouin distributed discrimination of strain and temperature using a polarization-maintaining optical fiber," Photonics Technology Letters, IEEE 22, 526-528 (2010).

[114] Y. Dong, L. Chen, and X. Bao, "High-spatial-resolution time-domain simultaneous strain and temperature sensor using Brillouin scattering and birefringence in a polarization-maintaining fiber," Photonics Technology Letters, IEEE 22, 1364-1366 (2010).

[115] R. K. Yamashita, W. Zou, Z. He, and K. Hotate, "Measurement range elongation based on temporal gating in Brillouin optical correlation domain distributed simultaneous sensing of strain and temperature," Photonics Technology Letters, IEEE 24, 1006-1008 (2012).

[116] W. Zou, Z. He, and K. Hotate, "Range Elongation of Distributed Discrimination of Strain and Temperature in Brillouin Optical Correlation-Domain Analysis Based on Dual Frequency Modulations," Sensors Journal, IEEE 14, 244-248 (2014).

[117] R. K. Yamashita, H. Zuyuan, and K. Hotate, "Spatial Resolution Improvement in Correlation Domain Distributed Measurement of Brillouin Grating," Photonics Technology Letters, IEEE 26, 473-476 (2014).

[118] X. Bao, J. Dhliwayo, N. Heron, D. J. Webb, and D. A. Jackson, "Experimental and theoretical studies on a distributed temperature sensor based on Brillouin scattering," Lightwave Technology, Journal of 13, 1340-1348 (1995).

[119] J. Smith, A. Brown, M. DeMerchant, and X. Bao, "Pulse width dependance of the Brillouin loss spectrum," Opt. Commun. 168, 393-398 (1999).

[120] A. W. Brown, M. D. DeMerchant, X. Bao, and T. W. Bremner, "Spatial resolution enhancement of a Brillouin-distributed sensor using a novel signal processing method," J. Lightwave Technol. 17, 1179 (1999).

[121] K. Kishida, C. Li, S. Lin, and K. I. NISHIGUCHI, "Pulse pre-pump method to achieve cm-order spatial resolution in Brillouin distributed measuring technique," Technical report of IEICE, 15-20 (2004).

[122] S. Afshar V, G. A. Ferrier, X. Bao, and L. Chen, "Effect of the finite extinction ratio of an electro-optic modulator on the performance of distributed probe-pump Brillouin sensorsystems," Opt. Lett. 28, 1418-1420 (2003).

[123] A. W. Brown, B. G. Colpitts, and K. Brown, "Distributed sensor based on dark-pulse Brillouin scattering," Photonics Technology Letters, IEEE 17, 1501-1503 (2005).

[124] A. W. Brown, B. G. Colpitts, and K. Brown, "Dark-pulse Brillouin optical time-domain sensor with 20-mm spatial resolution," J. Lightwave Technol. 25, 381-386 (2007).

[125] F. Wang, X. Bao, L. Chen, Y. Li, J. Snoddy, and X. Zhang, "Using pulse with a dark base to achieve high spatial and frequency resolution for the distributed Brillouin sensor," Opt. Lett. 33, 2707-2709 (2008).

[126] K. Y. Song, S. Chin, N. Primerov, and L. Thévenaz, "Time-domain distributed fiber sensor with 1 cm spatial resolution based on Brillouin dynamic grating," J. Lightwave Technol. 28, 2062-2067 (2010).

[127] K. Y. Song and H. J. Yoon, "High-resolution Brillouin optical time domain analysis based on Brillouin dynamic grating," Opt. Lett. 35, 52-54 (2010).

[128] S. Chin, N. Primerov, and L. Thevenaz, "Sub-centimeter spatial resolution in distributed fiber sensing based on dynamic Brillouin grating in optical fibers," Sensors Journal, IEEE 12, 189-194 (2012).

[129] W. Li, X. Bao, Y. Li, and L. Chen, "Differential pulse-width pair BOTDA for high spatial resolution sensing," Opt. Express 16, 21616-21625 (2008).

[130] Y. Dong, X. Bao, and W. Li, "Differential Brillouin gain for improving the temperature accuracy and spatial resolution in a long-distance distributed fiber sensor," Appl. Optics 48, 4297-4301 (2009).

[131] Y. Dong, H. Zhang, L. Chen, and X. Bao, "2 cm spatial-resolution and 2 km range Brillouin optical fiber sensor using a transient differential pulse pair," Appl. Optics 51, 1229-1235 (2012).

[132] A. Minardo, R. Bernini, and L. Zeni, "Differential techniques for high-resolution BOTDA: an analytical approach," Photonics Technology Letters, IEEE 24, 1295-1297 (2012).

[133] S. Foaleng-Mafang, J.-C. Beugnot, and L. Thévenaz, "Optimized configuration for high resolution distributed sensing using Brillouin echoes," in *20th International Conference on Optical Fibre Sensors*, (International Society for Optics and Photonics, 2009), 75032C-75032C-75034.

[134] S. M. Foaleng, M. Tur, J.-C. Beugnot, and L. Thévenaz, "High spatial and spectral resolution long-range sensing using Brillouin echoes," J. Lightwave Technol. 28, 2993-3003 (2010).

[135] Y. Koyamada, Y. Sakairi, N. Takeuchi, and S. Adachi, "Novel technique to improve spatial resolution in Brillouin optical time-domain reflectometry," Photonics Technology Letters, IEEE 19, 1910-1912 (2007).

[136] Y. Yao, Y. Lu, X. Zhang, F. Wang, and R. Wang, "Reducing Trade-Off Between Spatial Resolution and Frequency Accuracy in BOTDR Using Cohen's Class Signal Processing Method," Photonics Technology Letters, IEEE 24, 1337-1339 (2012).

[137] F. Wang, W. Zhan, X. Zhang, and Y. Lu, "Improvement of spatial resolution for BOTDR by iterative subdivision method," J. Lightwave Technol. 31, 3663-3667 (2013).

[138] Y. T. Cho, M. N. Alahbabi, M. J. Gunning, and T. P. Newson, "Enhanced performance of long range Brillouin intensity based temperature sensors using remote Raman amplification," Meas. Sci. Technol. 15, 1548-1552 (2004).

[139] K. De Souza and T. P. Newson, "Signal to noise and range enhancement of a Brillouin intensity based temperature sensor," Opt. Express 12, 2656-2661 (2004).

[140] Y. T. Cho, M. N. Alahbabi, G. Brambilla, and T. P. Newson, "Distributed Raman amplification combined with a remotely pumped EDFA utilized to enhance the per-

formance of spontaneous Brillouin-based distributed temperature sensors," IEEE Photonics Technol. Lett. 17, 1256-1258 (2005).

[141] X. H. Jia, Y. J. Rao, L. A. Chang, C. Zhang, and Z. L. Ran, "Enhanced Sensing Performance in Long Distance Brillouin Optical Time-Domain Analyzer Based on Raman Amplification: Theoretical and Experimental Investigation," J. Lightwave Technol. 28, 1624-1630 (2010).

[142] S. Martin-Lopez, M. Alcon-Camas, F. Rodriguez, P. Corredera, J. D. Ania-Castanon, L. Thevenaz, and M. Gonzalez-Herraez, "Brillouin optical time-domain analysis assisted by second-order Raman amplification," Opt. Express 18, 18769-18778 (2010).

[143] M. A. Soto, G. Bolognini, and F. Di Pasquale, "Optimization of long-range BOTDA sensors with high resolution using first-order bi-directional Raman amplification," Opt. Express 19, 4444-4457 (2011).

[144] X. Angulo-Vinuesa, S. Martin-Lopez, P. Corredera, and M. Gonzalez-Herraez, "Raman-assisted Brillouin optical time-domain analysis with sub-meter resolution over 100 km," Opt. Express 20, 12147-12154 (2012).

[145] X. Angulo-Vinuesa, S. Martin-Lopez, J. Nuno, P. Corredera, J. D. Ania-Castanon, L. Thevenaz, and M. Gonzalez-Herraez, "Raman-Assisted Brillouin Distributed Temperature Sensor Over 100 km Featuring 2 m Resolution and 1.2 degrees C Uncertainty," J. Lightwave Technol. 30, 1060-1065 (2012).

[146] M. A. Soto, G. Bolognini, and F. Di Pasquale, "Analysis of optical pulse coding in spontaneous Brillouin-based distributed temperature sensors," Opt. Express 16, 19097-19111 (2008).

[147] M. A. Soto, G. Bolognini, F. Di Pasquale, and L. Thévenaz, "Long-range Brillouin optical time-domain analysis sensor employing pulse coding techniques," Measurement Science and Technology 21, 094024 (2010).

[148] M. A. Soto, G. Bolognini, F. Di Pasquale, and L. Thévenaz, "Simplex-coded BOTDA fiber sensor with 1 m spatial resolution over a 50 km range," Opt. Lett. 35, 259-261 (2010).

[149] M. A. Soto, P. K. Sahu, G. Bolognini, and F. Di Pasquale, "Brillouin-based distributed temperature sensor employing pulse coding," IEEE Sens. J. 8, 225-226 (2008).

[150] M. A. Soto, S. Le Floch, and L. Thevenaz, "Bipolar optical pulse coding for performance enhancement in BOTDA sensors," Opt. Express 21, 16390-16397 (2013).

[151] M. Taki, Y. Muanenda, C. J. Oton, T. Nannipieri, A. Signorini, and F. Di Pasquale, "Cyclic pulse coding for fast BOTDA fiber sensors," Opt. Lett. 38, 2877-2880 (2013).

[152] M. A. Soto, G. Bolognini, and F. D. Pasquale, "Long-range simplex-coded BOTDA sensor over 120km distance employing optical preamplification," Opt. Lett. 36, 232-234 (2011).

[153] M. A. Soto, M. Taki, G. Bolognini, and F. Di Pasquale, "Simplex-Coded BOTDA Sensor Over 120-km SMF With 1-m Spatial Resolution Assisted by Optimized Bidirectional Raman Amplification," IEEE Photonics Technol. Lett. 24, 1823-1826 (2012).

[154] F. Gyger, E. Rochat, S. Chin, M. Niklès, and L. Thévenaz, "Extending the sensing range of Brillouin optical time-domain analysis up to 325 km combining four optical repeaters," in *OFS2014 23rd International Conference on Optical Fiber Sensors*, (International Society for Optics and Photonics, 2014), 91576Q-91576Q-91574.

[155] R. Bernini, A. Minardo, and L. Zeni, "Long-range distributed Brillouin fiber sensors by use of an unbalanced double sideband probe," Opt. Express 19, 23845-23856 (2011).

[156] D. M. Nguyen, B. Stiller, M. W. Lee, J.-C. Beugnot, H. Maillotte, A. Mottet, J. Hauden, and T. Sylvestre, "Distributed Brillouin Fiber Sensor With Enhanced Sensitivity Based on Anti-Stokes Single-Sideband Suppressed-Carrier Modulation," IEEE Photonics Technol. Lett. 25, 94-96 (2013).

[157] K. Hotate, K. Abe, and K. Y. Song, "Suppression of signal fluctuation in Brillouin optical correlation domain analysis system using polarization diversity scheme," IEEE Photonics Technol. Lett. 18, 2653-2655 (2006).

[158] K. Y. Song and K. Hotate, "Enlargement of measurement range in a Brillouin optical correlation domain analysis system using double lock-in amplifiers and a single-sideband modulator," IEEE Photonics Technol. Lett. 18, 499-501 (2006).

[159] J. H. Jeong, K. Lee, K. Y. Song, J. M. Jeong, and S. B. Lee, "Variable-frequency lock-in detection for the suppression of beat noise in Brillouin optical correlation domain analysis," Opt. Express 19, 18721-18728 (2011).

[160] K. Y. Song, Z. He, and K. Hotate, "Optimization of Brillouin optical correlation domain analysis system based on intensity modulation scheme," Opt. Express 14, 4256-4263 (2006).

[161] K. Y. Song, Z. Y. He, and K. Hotate, "Effects of intensity modulation of light source on Brillouin optical correlation domain analysis," J. Lightwave Technol. 25, 1238-1246 (2007).

[162] J. H. Jeong, K. Lee, K. Y. Song, J. M. Jeong, and S. B. Lee, "Differential measurement scheme for Brillouin Optical Correlation Domain Analysis," Opt. Express 20, 27094-27101 (2012).

[163] M. Kannou, S. Adachi, and K. Hotate, "Temporal gating scheme for enlargement of measurement range of Brillouin optical correlation domain analysis for optical fiber distributed strain measurement," in *Proc. 16th Int. Conf. Optical Fiber Sensors*, 2003), 454-457.

[164] K. Hotate and H. Arai, "Enlargement of measurement range of simplified BOCDA fiber-optic distributed strain sensing system using a temporal gating scheme," in *Brug-*

es, Belgium-Deadline Past, (International Society for Optics and Photonics, 2005), 184-187.

[165] Y. Mizuno, Z. He, and K. Hotate, "Measurement range enlargement in Brillouin optical correlation-domain reflectometry based on temporal gating scheme," Opt. Express 17, 9040-9046 (2009).

[166] Y. Mizuno, Z. Y. He, and K. Hotate, "Measurement range enlargement in Brillouin optical correlation-domain reflectometry based on double-modulation scheme," Opt. Express 18, 5926-5933 (2010).

[167] D. Elooz, Y. Antman, N. Levanon, and A. Zadok, "High-resolution long-reach distributed Brillouin sensing based on combined time-domain and correlation-domain analysis," Opt. Express 22, 6453-6463 (2014).

[168] A. Denisov, M. A. Soto, and L. Thévenaz, "1'000'000 resolved points along a Brillouin distributed fibre sensor," in *OFS2014 23rd International Conference on Optical Fiber Sensors*, (International Society for Optics and Photonics, 2014), 9157D9152-9157D9152-9154.

[169] A. Zadok, Y. Antman, N. Primerov, A. Denisov, J. Sancho, and L. Thevenaz, "Random-access distributed fiber sensing," Laser Photon. Rev. 6, L1-L5 (2012).

[170] W. Zou, Z. He, and K. Hotate, "Distributed dynamic-strain sensing based on brillouin optical correlation domain analysis," in *Lasers & Electro Optics & The Pacific Rim Conference on Lasers and Electro-Optics, 2009. CLEO/PACIFIC RIM'09. Conference on*, (IEEE, 2009), 1-2.

[171] W. Zou, Z. He, and K. Hotate, "Realization of high-speed distributed sensing based on Brillouin optical correlation domain analysis," in *Conference on Lasers and Electro-Optics*, (Optical Society of America, 2009),

[172] K. Y. Song, M. Kishi, Z. Y. He, and K. Hotate, "High-repetition-rate distributed Brillouin sensor based on optical correlation-domain analysis with differential frequency modulation," Opt. Lett. 36, 2062-2064 (2011).

[173] K. Hotate and S. S. L. Ong, "Distributed dynamic strain measurement using a correlation-based brillouin sensing system," IEEE Photonics Technol. Lett. 15, 272-274 (2003).

[174] K. Y. Song and K. Hotate, "Distributed fiber strain sensor with 1-kHz sampling rate based on Brillouin optical correlation domain analysis," IEEE Photonics Technol. Lett. 19, 1928-1930 (2007).

[175] T. Yamauchi and K. Hotate, "Distributed and dynamic strain measurement by BOCDA with time-division pump-probe generation scheme," in *Conference on Lasers and Electro-Optics*, (Optical Society of America, 2004),

[176] Y. Mizuno, Z. Y. He, and K. Hotate, "One-End-Access High-Speed Distributed Strain Measurement with 13-mm. Spatial Resolution Based on Brillouin Optical Correlation-Domain Reflectometry," IEEE Photonics Technol. Lett. 21, 474-476 (2009).

IntechOpen

IntechOpen